UNIVERSITY OF CALIFORNIA
RIVERSIDE

A Comprehensive Study of the Rest-UV Properties of Dwarf Galaxies During the Epoch of Peak Star Formation

A Dissertation submitted in partial satisfaction
of the requirements for the degree of

Doctor of Philosophy

in

Physics

by

Christopher Robert Snapp-Kolas

June 2023

Dissertation Committee:

Dr. Brian Siana, Chairperson
Dr. Simeon Bird
Dr. George Becker

The Dissertation of Christopher Robert Snapp-Kolas is approved:

Committee Chairperson

University of California, Riverside

Acknowledgments

First and foremost I must acknowledge the creator of this wonderful universe. It is a great privilege to have the ability to inquire, study, and understand the inner workings of a wonderfully complex creation. What little I have added to our understanding of our universe I pray brings honor to the God of all things.

Graduate school is a challenging endeavor that has been a trial unlike anything else in my life and many things in my life have changed since I started this journey. I am continually grateful to my family who have believed in my abilities to accomplish this goal even when I did not believe I could. My Father, Roy Snapp-Kolas, with whom I have had many a philosophical discussion, I thank for giving me clarity of thought. You have been a refuge for my mind. My Mother, Sharon Snapp-Kolas, I thank for understanding the emotional and mental difficulties associated with regularly editing work and coming up against walls. You have been a refuge for my soul. My brother, Joshua Kolas, I thank for being on my side and listening to me vent my frustrations in the process. You have been a refuge for my heart.

During my time at UCR I have made friends with other graduate students with whom I was able to endure through graduate school with. In particular, I thank Timothy Gburek, Jessica Doppel, Ryan Vo, Reza Monadi, Archana Aravindan, and Nakul Gongoli. You have all helped me to realize we are all stronger and more capable than we think.

I wish to thank my advisor, Dr. Brian Siana, who has encouraged me all along the way to write this work. His advice, edits, and teaching have helped me to become a capable researcher, and to understand better the field of observational astronomy. I cannot

express here the degree to which his input has improved my abilities to comprehend and navigate the vast ocean of scientific work in the literature.

Finally, I wish to thank all the friends I have made over the past 2 years at Sandals Church Moreno Valley. You all have become family to me. I want to especially mention Adrian Monroy, Nicolas Munoz, and Bryan Schutte who all helped me through some of the darkest moments of my life. I cannot express how grateful I am for each of you and how blessed I am to know you. I also want to thank Miguel Soto, Micheal Soto, Lucius Phan, Ed Wimpenny, Eric Schessler, Kayla McKinney, Pastor Andrew Bogenwright, Nicole Centofranchi, and many more from the worship and production teams. I am a stronger and better person for knowing all of you.

I wish to thank the developers of the `PypeIt` data reduction pipeline. Particulary Xavier Prochaska, Joseph Hinnawi, and Kyle Westfield who regularly helped clarify the intricacies of the code. I would also like to thank the developers of `BAGPIPES` which allowed for additional galaxies to be added into our stacking sample to improve the S/N of the stack.

A portion of this dissertation is an early printing of papers submitted for publication with the *Monthy Notices of the Royal Astronomical Society.*

ABSTRACT OF THE DISSERTATION

A Comprehensive Study of the Rest-UV Properties of Dwarf Galaxies During the Epoch of Peak Star Formation

by

Christopher Robert Snapp-Kolas

Doctor of Philosophy, Graduate Program in Physics
University of California, Riverside, June 2023
Dr. Brian Siana, Chairperson

Galaxy evolution is concerned with the mechanisms that determine the distributions of gas, dust, and metals, and with the efficiency with which galaxies produce stars. These components are the primary visible building blocks of a galaxy. Throughout cosmic history the escape of ionizing radiation from a galaxy out into the intergalactic medium has been a notoriously difficult measurement to make, and one that informs the ionizing background radiation. This is relevant for the development of galaxies generally, but also plays a significant role in understanding the last great phase change of the universe, reionization ($z \sim 6$). It is unclear whether it is massive galaxies or dwarf galaxies which are able to expel sufficient amounts of ionizing radiation to ionize neutral hydrogen in the intergalactic medium during this epoch of the universe. Any attempts to measure the ionizing escape fraction during reionization is untenable even for newer instruments like the James Webb space telescope due to the neutral intergalactic medium obscuring large amounts of ionizing radiation. As such, lower redshift galaxies are studied both for the sake of constraining the ionizing background throughout cosmic history and as benchmarks for understanding

reionization. Often, studies will select galaxies based on their Lyα emission as it has a possible connection with Lyman continuum escape. However, since Lyα is a resonant line transition it is absorbed and scattered by even small amounts of neutral hydrogen. Because of this, it is unclear what galaxy properties may be correlated with Lyα escape. To understand the biases behind selecting on Lyα we need to better understand what causes Lyα to escape and the distribution of Lyα properties in galaxy samples. Lyα also serves as a proxy of the neutral fraction in the intergalactic medium at high redshift. Finally, outflows and feedback are best understood by comparing empirical measures of outflows and covering fractions with models from simulations. These models can be better constrained when including empirical markers in the dwarf regime. Many studies have looked into these measurements at higher masses ($\log(M^*/M_\odot) > 9$), or for samples biased towards strong line emitters. There has yet to be a complete sample of low mass galaxies studied at $z \sim 2$.

In this work we present a sample of 32 galaxies at $z \sim 2$ during the peak of star-formation in the history of the universe. We focus on low-UV luminosity ($M_{UV} > -19$) and low mass ($\log(M^*/M_\odot) < 9$) sub-samples of this parent sample. A unique characteristic of this sample is the complete spectroscopy of the galaxies. Each galaxy has rest-UV and rest-optical spectra from the Keck/LRIS and keck/MOSFIRE instruments respectively. This allows us to confirm the redshift of galaxies for which we do not observe any apparent spectral features in the rest-UV spectra. This, along with improved S/N from gravitational lensing, allows us to to produce a complete sample of dwarf galaxies from which to measure proxies of the ionizing escape fraction of galaxies. The primary proxies used in the literature

and in this work are the Lyα EW, the Lyα escape fraction, and the low-ionization interstellar absorption line EW (Saldana-Lopez et al. 2023).

The Lyα EW we measure for individual galaxies and find that generally dwarf galaxies tend to have Lyα in emission in contrast to higher mass samples which show Lyα EWs have Lyα in absorption on average (Du et al. 2018). The volumetric escape fraction of dwarf galaxies at $z \sim 2$ is consistent with the literature value of 5% (Hayes et al. 2010; Ciardullo et al. 2014; Sobral et al. 2017; Weiss et al. 2021), placing an upper limit on the volumetric escape fraction of ionizing photons. The LIS absorption lines show about a factor of 2 weaker EWs for low mass galaxies when compared with higher mass samples (Jones et al. 2012; Du et al. 2018). A lower EW of LIS absorption lines implies a lower covering fraction of neutral hydrogen and therefore greater avenues of escape on average for ionizing photons. Collectively, our measurements imply greater amounts of ionizing radiation escaping from dwarf galaxies on average when compared with higher mass samples of star-forming galaxies.

Contents

List of Figures

Chapter 1

Introduction

The evolution of galaxies throughout cosmic history is dependent on the supply of radiation, hydrogen/metal-enriched gas, and dust. The distribution and availability of these various components of the visible universe are interdependent in complex ways that we seek to understand in order to constrain the properties of ionizing radiation and the star-formation efficiencies of galaxies. The rest-UV spectroscopy of galaxies provide a rich source of information for understanding ionizing radiation, gas, and dust.

As galaxies start to form and evolve they are often surrounded by large quantities of gas and dust that mitigate the escape of hydrogen ionizing radiation. The amount of ionizing radiation that galaxies expel into the intergalactic medium (IGM) is a key constraint on the ionizing background radiation during all epochs of the universe, and in particular constrains the ability of galaxies to ionize the neutral hydrogen of the IGM during the "dark ages" and into reionization. There are two primary ways in which a galaxy can modulate the amount of ionizing radiation it sends into the IGM. First, through the stellar

populations. The stellar populations of a given galaxy could in principle produce copious amounts of ionizing radiation. If there are more numerous stellar sources of this sort, then the galaxy can expel more ionizing photons into the IGM. Second, through the distribution of intervening gas. Neutral hydrogen absorbs ionizing radiation quite strongly. If there is a screen of sufficiently high column density hydrogen gas in front of the stellar populations producing ionizing photons, then those photons will not escape into the IGM. A model gaining popularity in the literature is the picket fence model, first proposed more than a decade ago using the cosmic horseshoe (Quider et al. 2009). In this model, a star-forming region is surrounded by high column density gas with holes of low column density gas that allows the escape of ionizing radiation. Likely, a combination of these two are at play in every galaxy, but we wish to understand to what extent and what proxies there are for these physical phenomena. In particular, we are interested in these proxies in dwarf galaxies.

According to the luminosity functions of Alavi et al. (2016), Konno et al. (2016), and Bouwens et al. (2022) dwarf galaxies are the most plentiful galaxies in the universe at $z \sim 2$ and become even more plentiful at higher redshifts. Due to the low-potential wells of these galaxies they may be more likely to expel large amounts of gas, particularly due to the typical bursty nature of the star-formation histories of these galaxies (e.g. Sparre et al. 2017; Emami et al. 2021). This makes it likely that these galaxies will have higher amounts of ionizing photons escaping and may serve to elucidate our understanding of feedback in low-mass halos. Furthermore, Senchyna et al. (2017) demonstrate that the ionizing photon production efficiency is greater in lower mass galaxies. Because of these unique properties

of dwarf galaxies it is particularly important to understand the escape of ionizing radiation and the covering fraction of neutral hydrogen in these sources.

To measure the ionizing radiation directly is incredibly difficult often requiring long integration times (e.g. Vanzella et al. 2012) or stacks of many galaxies (e.g. Leitet et al. 2013). The primary issue is that ionizing radiation interacts so strongly with neutral hydrogen which is the most abundant element of the universe. During and before the epoch of reionization it may not be possible to directly observe the escape of ionizing radiation except in the most extreme cases of large ionization bubbles. It is also difficult to measure directly the distribution of neutral hydrogen gas at high redshift given the spatial and spectral resolution limits of many detectors. As such we make use of proxies to quantify the output of ionizing radiation from stellar sources and the attenuation of ionizing radiation through gas and dust.

One of the primary proxies for ionizing radiation and the distribution of neutral gas is the Lyα emission line. This emission line was first proposed as a tracer of distant galaxies in the 1960's (Partridge & Peebles 1967) and has gained added uses over time. Since Lyα is a resonant line transition it is more sensitive to the presence of neutral hydrogen than the ionizing radiation. As such, any escape of Lyα radiation implies very low column densities of neutral hydrogen and therefore may imply the escape of ionizing radiation along the same sight line. Some works in the literature have demonstrated this concept (e.g. Verhamme et al. 2015; Dijkstra et al. 2016). Many studies have looked at the Lyα escape fraction, and the Lyα equivalent width, as proxies either of the escape fraction of ionizing radiation or of the covering fraction of neutral hydrogen for high mass ($\log(M^*/M_\odot) > 9$ galaxies or

galaxies selected to have strong Lyα radiation (e.g. Berry et al. 2012; Konno et al. 2016; Sobral et al. 2017; Du et al. 2018; Sobral & Matthee 2019; Hashimoto et al. 2017; Gronwall et al. 2007; Guaita et al. 2010; Adams et al. 2011). However, several studies have shown that contributions from lower mass galaxies may be significant, and grow in significance with redshift (e.g. Alavi et al. 2016). This low-mass parameter space remains mostly unexplored.

Another proxy of the covering fraction of neutral hydrogen is the equivalent width of the low-ionization interstellar absorption lines. These absorption features present in the rest-UV spectra of galaxies are the result of UV continuum radiation being obscured by the presence of metals such as silicon and carbon. Singly ionized silicon and carbon have ionization potentials below that of neutral hydrogen and therefore are quickly ionized by hard radiation from star-forming regions. In order to persist these ions primarily exist within regions of dense hydrogen gas where they are protected from hard radiation. As such, these metals can trace the distribution of neutral hydrogen gas. Several studies of higher mass galaxies have looked at the connection between the presence of low-ionization interstellar absorption and ionizing radiation (e.g. Trainor et al. 2019; Saldana-Lopez et al. 2022). But little has been done for lower mass samples of galaxies.

We present in this work the rest-UV spectroscopy of a complete sample of dwarf galaxies at $z \sim 2$. We have obtained rest-UV and rest-optical spectroscopy from the Keck/LRIS and Keck/MOSFIRE telescopes respectively. In addition to this we have photometry from the Hubble space telescope. These observations probe to the faintest absolute UV magnitudes ($M_{UV} < -17$) possible with spectroscopy at this redshift. This is possible through the use of lensing clusters which magnify background galaxies achromatically.

We will compare our sample of dwarf galaxies with higher mass samples to demonstrate any changes in the Lyα escape fraction, the Lyα equivalent width, or the low-ionization absorption line equivalent width.

In chapter 2, we investigate the Lyman alpha equivalent width ($EW_{Ly\alpha}$) distribution for a complete sample of dwarf galaxies at $z \sim 2$. With access to both rest-UV and rest-optical spectroscopy, as well as space-based photometry, we are able to get a complete spectroscopic picture of these lensed dwarf galaxies. With two subsamples of dwarf galaxies we investigate stellar populations and ISM properties through the intrinsic Lyα EW and Lyα escape fraction respectively. The measurements are compared with the higher UV luminosity samples of KBSS (Du et al. 2018, 2021) and VUDS (Le Fèvre et al. 2015; Hathi et al. 2016; Cassata et al. 2015) at $z \sim 2$ to identify any trends in $EW_{Ly\alpha}$ with UV luminosity. We also compare our intrinsic $EW_{Ly\alpha}$ with the measurements of Shivaei et al. (2018) and Emami et al. (2020) who measure the ionizing photon production efficiency (ξ_{ion}) which differs from $EW_{Ly\alpha}$ by a multiplicative factor. This type of galaxy is often suggested as a source of reionization and so we also measure 1) The volumetric Lyα escape fraction and 2) the fraction of Lyα emitters (X_{LAE}) as these quantities are indicative of the amount of ionizing photon escape (e.g. Matthee et al. 2021a) and the IGM neutral fraction (Stark et al. 2010, 2011; Pentericci et al. 2011; Curtis-Lake et al. 2012; Ono et al. 2012; Schenker et al. 2012; Cassata et al. 2015; De Barros et al. 2017; Haro et al. 2018; Caruana et al. 2018; De La Vieuville et al. 2020; Kusakabe et al. 2020; Zhang et al. 2021) respectively.

In chapter 3, we investigate the properties of the ISM through the LIS and HIS absorption lines in the rest-UV spectroscopy. Our measurements have too little S/N to

measure the absorptuon features in individual galaxies, so we stack our sample of dwarf galaxies to get a measure of the typical dwarf galaxy at $z \sim 2$. We compare primarily with the sample of Du et al. (2018) who stack UV spectra of galaxies at various redshfits, including $z \sim 2$ to investigate any trends in rest-UV spectroscopic measurements with redshift. We also compare with other higher redshift samples from Jones et al. (2012), Sugahara et al. (2019), and Harikane et al. (2020). We investigate the kinematics of the HIS and LIS absorption lines, there relationship to $\mathrm{EW}_{\mathrm{Ly}\alpha}$, and any possible trends with mass and UV luminosity. In chapter 4, we summarize and discuss the results of the preceding chapters and look to the future of studies of the faint universe and possible observations with new and upcoming telescopes such as the James Webb space telescope (JWST) and the thirty-meter telescope (TMT).

Chapter 2

Paper I: The Origin of the Observed Lyα EW Distribution of Dwarf Galaxies at $z \sim 2$[1]

abstract: We present a rest-UV selected sample of 32 lensed galaxies at $z \sim 2$ observed with joint Keck/LRIS rest-UV and Keck/MOSFIRE rest-optical spectra behind the clusters Abell 1689, MACS J0717, and MACS J1149. The sample pushes towards the faintest UV luminosities observed ($-19 \leq \mathrm{M_{UV}} \leq -17$) at this redshift. The fraction of dwarf galaxies identified as Lyα emitters (EW ≥ 20 Å) is $\mathrm{X_{LAE}} = 33^{+17}_{-12}\%$. We use the Balmer lines and UV

[1]This chapter contains a draft of an article that has been accepted for publication by the Monthly Notices of the Royal Astronomical Society written by C. Snapp-Kolas, B. Siana, T. Gburek, A. Alavi, N. Emami, J. Richard, D.P. Stark, C. Scarlata, B.C. Lemaux, G. Zamorani, S. Bardelli, N. Hathi, and P. Cassata

continuum to estimate the *intrinsic* EW allowing us to distinguish the effects of the ionizing spectra and escape fraction on the observed EW distribution. Fainter galaxies ($M_{UV} > -19$) show larger intrinsic EWs and escape fractions than brighter galaxies. Only galaxies with intrinsic EWs greater than 40 Å have escape fractions larger than 5%. We find an anti-correlation between the escape fraction and A_V as well as UV spectral slope. The volumetric escape fraction of our sample is $f_{esc}^{Ly\alpha} = 4.6^{+2.0}_{-1.4}\%$ in agreement with measurements found elsewhere in the literature. 60% of the total integrated Lyα luminosity density comes from galaxies with $EW_{obs} > 20$ Å.

galaxies: evolution – galaxies: high-redshift

2.1 Introduction

More than five decades ago, Lyα was proposed as a tracer of early stage star forming galaxies (Partridge & Peebles 1967). Since then Lyα has been used to study star-forming galaxies locally and at the highest redshifts observed (e.g. Shapley et al. 2003; Jung et al. 2020). It has been used to study reionization (Bolton & Haehnelt 2013; Mesinger et al. 2015; Mason et al. 2018; Matthee et al. 2021b), the interstellar medium (ISM, Du et al. 2021), the circumgalactic medium (Matsuda et al. 2012; Hayes et al. 2014), and has confirmed the redshifts of distant star-forming galaxies (Caruana et al. 2014; Hoag et al. 2019; Endsley et al. 2020; Jung et al. 2020).

Lyα is a resonant line and has a large cross section. Therefore, it will be scattered even by low column density gas. This makes it a great tracer of gas distributions, but can result in difficulties in interpreting observations. Furthermore, Lyα can be easily absorbed

by dust in the interstellar medium (ISM) reducing the strength of the line. Lyα observations are even more difficult when we try to observe galaxies during or before the epoch of reionization where there are large amounts of neutral hydrogen in the intergalactic medium (IGM) which can scatter whatever Lyα manages to escape. Each of these effects can drastically hamper the observability of Lyα and have strong effects on the distribution of observed Lyα equivalent widths (EWs) (Stark et al. 2010, 2011). In fact, at high redshift the attenuation of Lyα can be a useful probe of the neutral fraction of hydrogen in the intergalactic medium. But in order to measure the attenuation, one must first know the *intrinsic* distribution of $EW_{Ly\alpha}$ to compare with the observed distribution. The evolution of the $EW_{Ly\alpha}$ distribution has been used to study the end of reionization and is well understood from z= $3-6$ and for "bright" galaxies with absolute UV magnitudes $M_{UV} < -19$ (Stark et al. 2010, 2011; Pentericci et al. 2011; Curtis-Lake et al. 2012; Ono et al. 2012; Schenker et al. 2012; Cassata et al. 2015; De Barros et al. 2017; Haro et al. 2018; Caruana et al. 2018; De La Vieuville et al. 2020; Kusakabe et al. 2020; Zhang et al. 2021). At $z = 2$ there has been some study of the brighter star-forming galaxies ($M_{UV} < -19$) (Reddy & Steidel 2009; Cassata et al. 2015; Hathi et al. 2016; Du et al. 2021; Zhang et al. 2021), but little work has been done to study the fainter population ($M_{UV} > -19$). However, according to the luminosity functions of Alavi et al. (2016), Konno et al. (2016), and Bouwens et al. (2022) the faint galaxy population is larger at $z = 2$ and becomes more numerous with redshift. Therefore, if we want to understand reionization we need more information on the faint galaxy population, and $z = 2$ galaxies can help to constrain the $EW_{Ly\alpha}$ distribution at higher redshift where observation of Lyα is more difficult.

Lyα studies will often select galaxies via their rest-UV continuum luminosity density (via broadband imaging), or their Lyα line emission (via narrowband imaging, Berry et al. 2012; Konno et al. 2016; Sobral et al. 2017; Sobral & Matthee 2019; Hashimoto et al. 2017). Narrow-band selected samples will be biased towards Lyα emitters (LAEs) as they typically require $EW^{rest}_{Ly\alpha} > 20$ Å for a galaxy to be detected (e.g. Gronwall et al. 2007; Guaita et al. 2010; Adams et al. 2011). Alternatively, narrow-band studies of Lyα often select on other emission lines in the optical (such as [OIII]5007) (e.g. Ciardullo et al. 2014; Weiss et al. 2021). Erb et al. (2016) show that [OIII]5007-selected galaxies are biased towards LAEs by comparing the fraction of LAEs (X_{LAE}) in their [OIII]5007 selected sample with a sample of UV-selected galaxies. 80% are found to be LAEs in their [OIII]5007 sample while only 9% are found to be LAEs in their UV selected sample. This is further confirmed in Trainor et al. (2019) and Weiss et al. (2021), indicating that samples selected on nebular emission lines are biased toward Lyα emission. A sample chosen irrespective of the strength of nebular emission lines would be useful for understanding the full distribution of Lyα EWs. With an unbiased sample, it is possible to disentangle the effects of the stellar population (e.g. age and metallicity) and that of the gas and dust on the observed EW distribution. Broad-band surveys, which select galaxies independent of emission line strength, are able to probe down to $R_{AB} \sim 30$, but the followup spectroscopy necessary for accurate escape fraction and EW analyses limit the observations to $R_{AB} < 25.5$ (i.e Reddy et al. 2008) in order to obtain sufficient S/N in the continuum.

The Lyα EW distribution is dependent on the escape fraction of Lyα photons. Past studies have measured the Lyα escape fraction by comparing the Lyα luminosity den-

sity with the Ha or UV continuum luminosity densities, obtained by integrating luminosity functions (Hayes et al. 2010; Ciardullo et al. 2014; Konno et al. 2016). However, comparing luminosity densities does not allow for analysis of individual galaxy escape fractions or correlations with other properties of the population. Others make use of narrowband imaging of Lyα and one of the Balmer lines (e.g. Trainor et al. 2015) to make direct measurements of the Lyα escape fraction. Narrow-band imaging is biased towards high Lyα EW galaxies, and therefore does not represent the general population of star-forming galaxies as evidenced by the rather high average Lyα escape fractions of 30% (Kornei et al. 2010; Blanc et al. 2011; Wardlow et al. 2014; Trainor et al. 2015) which differs greatly from other measures with more complete samples (e.g. 5.3%, Hayes et al. 2010). Some try to model the escape fraction as a function of Lyα EW (e.g. Sobral & Matthee 2019), but this method must assume a star formation history and intrinsic ionizing continuum which are uncertain for low-mass galaxies. A direct measurement from a UV-selected sample with spectroscopic followup avoids these uncertainties.

What is needed is a measure of Lyα emission properties of a UV-selected sample of faint galaxies. We address this by selecting galaxies with photometric redshifts determined from HST photometry described in Alavi et al. (2014) and Alavi et al. (2016). We did not select on emission line flux and therefore the sample is unbiased towards Lyα emitters. Furthermore, by using gravitational lensing, we can study much fainter galaxies at $z = 2$. The goals of this paper are:

- Measure the Lyα EW distribution and determine its dependence on the properties of the ionizing sources and the Lyα escape fraction.

- Calculate the volumetric escape fraction of dwarf galaxies
- Identify trends in the EW distribution with absolute UV magnitude and redshift

The remainder of the paper is organized as follows. In §3.2, we discuss the observations, data reduction, and sample selection. In §2.3, we discuss fits to continua and emission lines, SED fitting, magnification, and dust estimates. In §3.3, we present our measured values of the EW distribution and the Lyα escape fraction. In §3.4, we discuss the implications of our measurements. In §3.5, we summarize the work. We adopt a ΛCDM cosmology with $\Omega_m = 0.3$, $\Omega_\Lambda = 0.7$, and $h = 0.7$ throughout the paper and all magnitudes are in the AB system (Oke & Gunn 1983). All EWs are reported in the rest-frame with the convention that positive EWs indicate emission. f_{esc} refers to the Lyα escape fraction throughout this paper.

2.2 Observations, Data Reduction, and Sample Selection

2.2.1 Observations & Data Reduction

Our sample consists of dwarf galaxies behind lensing clusters that have deep HST data and are accessible to the Keck Observatory (Abell 1689, MACS J1149, MACS J0717). Photometric redshifts were determined from HST photometry, as described in Alavi et al. (2014, 2016). Our selection criteria were photometric redshifts of $1.5 < z < 3.5$ and visual magnitudes brighter than $m_{F625W} < 26.3$. Slit allocation preference was given to galaxies with high magnification and photometric redshifts where the rest-optical lines are accessible in the YJHK atmospheric bands. In order to study physical properties (i.e. metallicity, $f_{\rm esc}$,

ionization parameter, etc.) of these dwarf galaxies we obtained Keck/MOSFIRE (McLean et al. 2010, 2012) spectra as described in Gburek et al. (2019). We also obtained Keck/LRIS optical spectra (Oke et al. 1995), for which the details are listed in Table 1. We observe eleven masks in three clusters with LRIS. Exposure times varied greatly (from 4500s-18000s) depending on the conditions and priority of objects in the mask, and seeing was typically $\sim 1''$. We decreased read noise by binning by 2 in the spectral direction of the CCD. We observed Macsj1149_1 on two seperate nights and have named the second night Macsj1149_1_2 in table 3.1. The A1689_1 mask was not targeted properly and we cannot confirm that the objects observed in the slits are those that were targeted and so we do not consider that mask in this work.

Table 2.1: List of data acquired with Keck/LRIS. In order from left to right we have the mask name used, the number of spectra obtained in each mask, the exposure time in seconds, the modified julian date (MJD), and the seeing in arcseconds

Mask (Name)	Spectra (Number)	Exposure Time (s)	MJD	Seeing (arcsec)
A1689_1	15	18000	55325	0.9
A1689_3	16	12286	55981	0.9
Macsj0717	11	12600	55981	1.1
Macsj1149_1	16	5400	57042	1.1
Macsj0717_2	8	9000	57042	0.7
Macsj0717_1	8	9000	57042	0.9
A1689_4	10	9000	57042	1.4
Macsj1149_1_2	13	5400	57043	0.8
A1689_z1_1	12	12000	57043	0.8
Macsj1149_2	5	4500	57398	1.0
Macsj0717_3	8	6720	57398	0.7
Macsj1149_3	11	4860	57870	1.5
A1689_6	10	9600	57870	1.0

The data were reduced using a modified version of the PypeIt v1.x reduction pipeline (Prochaska et al. 2020). This pipeline performs bias subtraction, flat fielding,

cosmic ray rejection, wavelength calibration, sky subtraction, and extracts the 1D spectra. The 1D spectra are extracted using an optimal extraction b-spline fitting to the object profile along the spatial direction. The 1D spectra are then flux calibrated using the spectrum of a standard star. The 1D spectra from each frame are then combined using a weighted mean algorithm in PypeIt. We perform a final absolute flux normalization by scaling the spectra of compact bright continuum sources to the *Hubble* photometry. We take the median (per mask) of these and scale the remaining spectra according to this median. Most of our galaxies are faint and therefore may not have their continua well-detected in the 1D spectra, so the use of a median correction from bright continuum sources is necessary for the absolute calibration.

We correct for slit losses by convolving the Hubble images with a Gaussian such that point sources in the final images would have a Gaussian FWHM equal to the seeing. We then measure the total flux and the flux within the slit. We use the F435W and F475W bands of Hubble for the Abell 1689 and MACS J0717/MACS J1149 masks respectively. We apply this correction to our spectra, to obtain an estimate of the total flux, but refrain from applying the correction when displaying spectra. We do not account for possible offsets between the UV continuum and the Lyα emission line. By visual inspection of the 2D spectra we find only one galaxy in our sample with any offset and therefore expect insignificant correction to our measurements from spatial offsets (see Claeyssens et al. 2022, for a discussion of offsets). We also do not consider extended Lyα emission which is likely present at some level in our galaxies (e.g. Leclercq et al. 2017; Claeyssens et al. 2022). However, two qualities regarding extended Lyα emission suggest that consideration of this

emission would have little effect on the qualitative trends found in this work. 1) The physical source of extended Lyα emission is uncertain. If the source is radiation from cold accreting gas, flourescence, or emission from satellite galaxies, then it would seem unreasonable, physically, to include this flux in our measurements of the escape fraction and Lyα EW for this study which is concerned with sources of Lyα emission from the stellar populations of each galaxy. In fact, Lujan Niemeyer et al. (2022) suggest that the origin of extended Lyα emission originates outside of the galaxy itself. 2) If the extended emission originates from star-forming regions it should be included and could account for 2/3 of the total Lyα emission (Leclercq et al. 2017) if it is entirely produced from the star forming regions. Nevertheless, our comparisons with other works which do not account for this correction will be the same given the same correction will be applied to their values as well.

When we have spectra of the same galaxy in different masks, we combine them using an inverse variance weighted mean. Some of our galaxies are multiply imaged, but combining multiple images involves demagnifying the spectra before combining and results in a spectrum of arbitrary magnification. Furthermore, the uncertainties in the magnification of high magnification galaxies would result in large uncertainties in the flux with little gain in S/N. Therefore, we remove highly magnified images (according to the threshold described in §2.2) for the multiply imaged galaxies.

The LRIS slit masks use box slits to align the masks on bright stars in the field. Occasionally, the spectra of these alignment stars will contaminate nearby slits. As a result some of the slits near the alignment stars are rejected due to poor sky subtraction. After accounting for slits affected by nearby box slits, our final count of extracted 1D spectra is

127. After accounting for multiple images and spectra of individual galaxies our final parent sample comes to 89 galaxies. Each cluster takes up about one half of the LRIS detector. We place longslits on the remaining half of the detector and do not consider spectra from these longslits in this work. Because of this we have about half the number of spectra typically expected from an LRIS mask. We estimate the spectral resolution of our spectra given the slit width of our observations is $\sim 1''$ with a plate scale of $0.135''$/pix, however we have binned along the wavelength direction such that the effective plate scale is $0.27''$/pix. The wavelength spacing is ~ 2.18 Å pix^{-1}. So the resolution of our observations is R ~ 500 or $\Delta v \sim 600$ km s^{-1}. We show some example 1D spectra in figure 2.1.

2.2.2 Sub-Sample Selection

The remainder of the paper focuses on an analysis of the fraction of Lyα emitters (X_{LAE}) and the escape fraction of Lyα photons (f_{esc}). In order to measure X_{LAE} in an unbiased manner we need to select a sub-sample of galaxies for which we can identify galaxies with no Lyα emission. That is, a spectroscopic redshift can be measured independent of detection of the Lyα line. We call this sub-sample the X_{LAE} sample. In order to measure f_{esc} we must be able to measure Hα. This is a more stringent requirement which eliminates a greater number of galaxies from the parent sample and would result in greater uncertainty in X_{LAE} were we to impose this condition on all of our data. Therefore, we choose to create an additional sub-sample which we call the Hα sample.

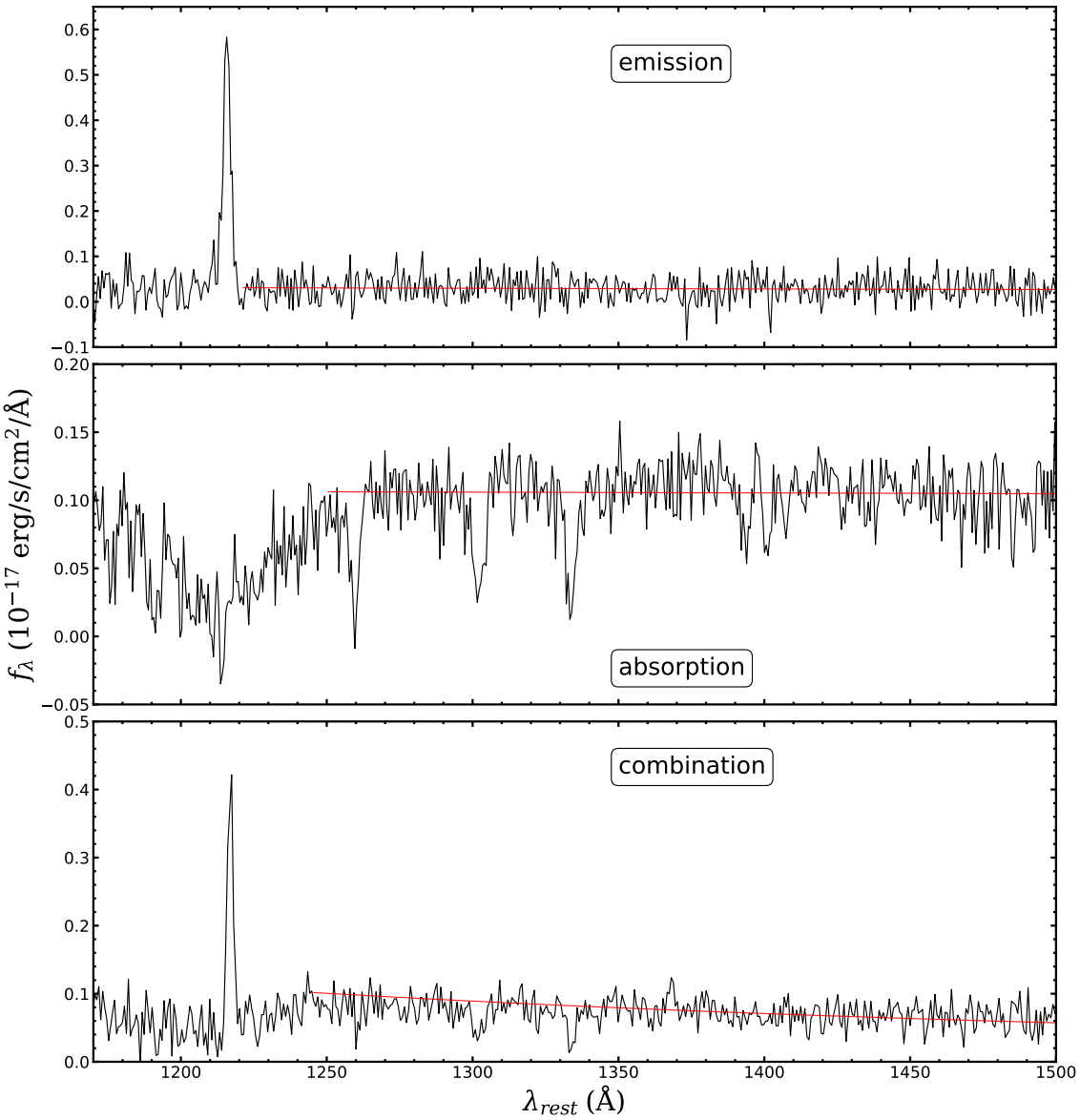

Figure 2.1: Three example spectra from our sample of galaxies. The red line is the continuum fit for each spectrum. The fitting method is described in section 2.3. Top: An example of an "emission" spectrum where we have Lyα in emission only. Middle: An example of an "absorption" spectrum. Bottom: An example of a "combination" spectrum where we see absorption and emission around Lyα

$\mathbf{X}_{\mathrm{LAE}}$ sample

We choose a sub-sample of galaxies from our sample of 89 in order to avoid biases in our Lyα equivalent width distribution. We account for biases from magnification, slit-losses, and possible blending of sources. We mimic the sub-sample selection methods of Emami et al. (2020), but with values derived from our sample as follows:

- We require secure redshifts for all the galaxies in this sample so that galaxies with no Lyα or Lyα in absorption can be identified. Therefore, only galaxies with confirmed redshifts from our MOSFIRE data are kept. These redshifts are primarily determined by Hα and [OIII]$\lambda\lambda$5007.

- We remove galaxies which do not have spectroscopic coverage of Lyα. Atmospheric absorption at $\lambda < 3200$ Å limits our analysis to galaxies at $z \gtrsim 1.6$.

- We remove galaxies for which there is possible confusion/blending with nearby objects in the slit. These objects could have emission lines from one galaxy and continuum from another, affecting the equivalent width measurements.

- We remove galaxies with large magnification, as they could suffer from differential magnification across the galaxy. This could introduce a bias into our sample which is selected on UV luminosity density. We therefore remove galaxies which have magnification $\mu > 30$ for Abell 1689 and $\mu > 15$ for MACS J0717 and MACS J1149.

- Finally, we remove galaxies with large slit loss correction in either LRIS or MOSFIRE. If a large fraction of the galaxy flux is outside of a slit, then it is not clear that a slitloss-corrected flux will reflect the true spectrum. Most of the galaxies have slit losses < 2.2

and we thus set this as our upper limit. The slit loss distributions are shown in figure 2.2.

After this cleaning of the sample we obtain a X_{LAE} sample of 32 galaxies with a mean redshift $\langle z \rangle = 2.27$.

Hα sample

In order to get a direct measurement of the Lyα escape fraction, Hα must be observable. Because of this we create a second sub-sample of galaxies from the X_{LAE} sub-sample for which Hα could have been observed, which limits the redshift range to $z \lesssim 2.6$. Additionally, the rest-UV HST data are very deep and the KECK Hα data are shallower which could bias us against galaxies that are faint in Hα. To check whether we are excluding galaxies that are too faint in Hα we calibrate our faint galaxy sample using our bright galaxies. We observe that our bright M_{UV} sample lies almost entirely above $\log(L_{H\alpha}/L_{UV}) \sim$ 13.4, as shown in figure 2.3, and therefore set this as our completeness limit for the sample. We take the median H$\alpha = 4.3 \times 10^{-18}$ erg s^{-1} cm^{-2} line flux error multiplied by 3 as our 3σ limit for detection of Hα. We then check our galaxies magnification and absolute UV magnitude and ask whether the galaxy would have been observable at $\log(L_{H\alpha}/L_{UV}) \sim$ 13.4. If the galaxy would not have been observable at 3σ at our completeness limit it was then removed. No galaxy fell below this criterion and therefore none were removed as shown in figure 2.3. We split our sample at $M_{UV} = -19$ and measure the mean and error on the mean of the bright and faint samples to be $\log(L_{H\alpha}/L_{UV}) = 13.5 \pm 0.1$ and $\log(L_{H\alpha}/L_{UV}) = 13.7 \pm 0.1$ respectively. While all but one of our galaxies have $\log(L_{H\alpha}/L_{UV}) > 13.4$, 11 of the

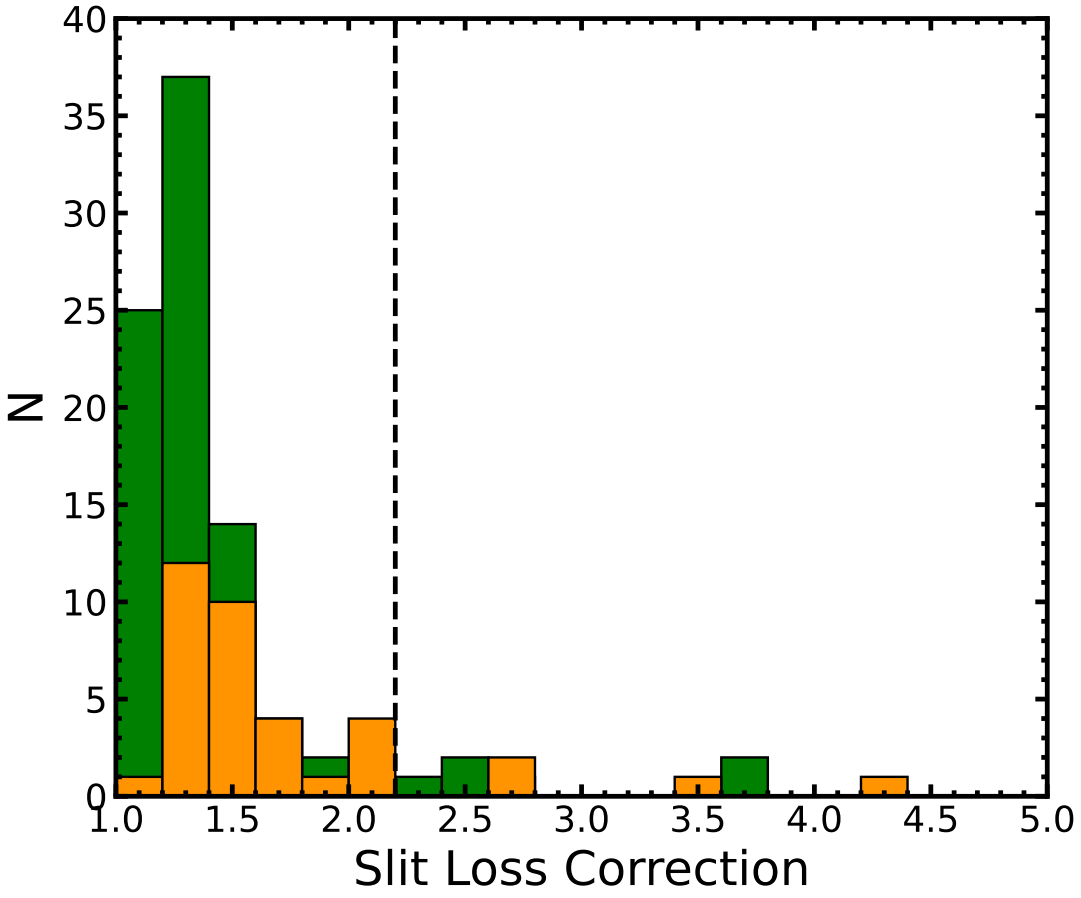

Figure 2.2: The distribution of slit loss corrections to our Hα (yellow) and Lyα (green) spectra. The dashed line at 2.2 denotes the upper limit we set for including galaxies in our sample.

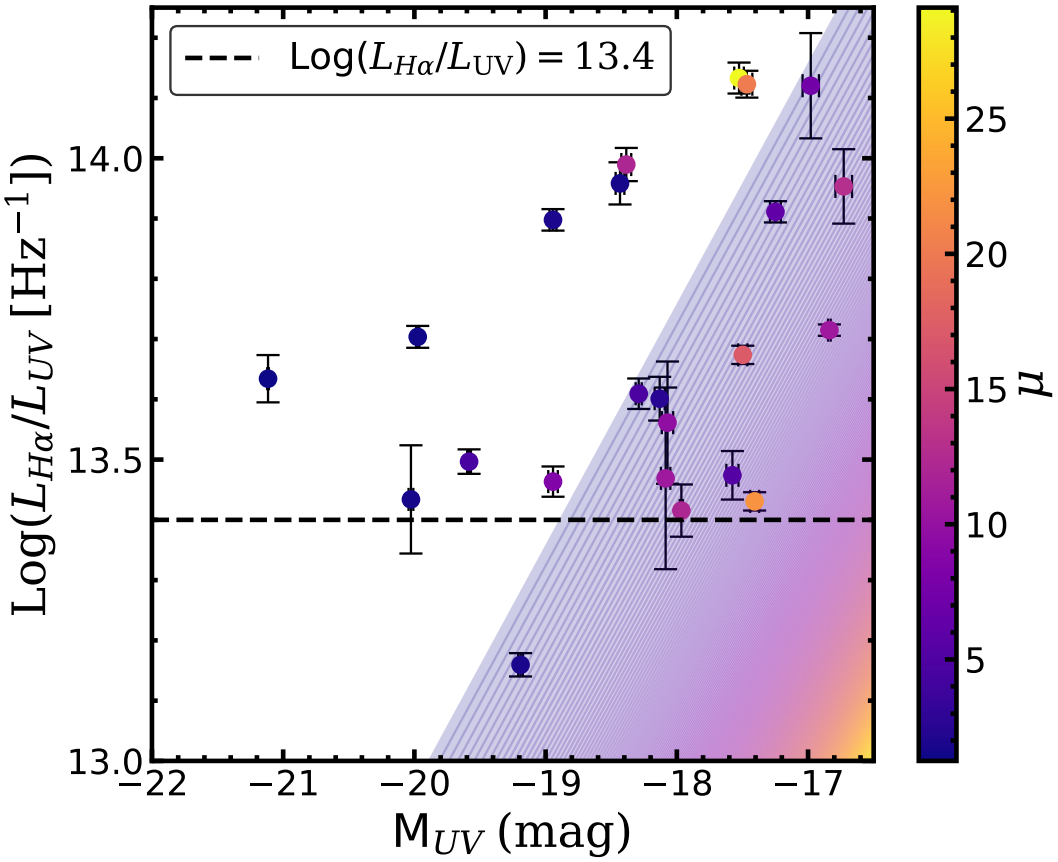

Figure 2.3: Plotted is the log($L_{H\alpha}/L_{UV}$) vs. delensed absolute UV magnitude. Points are color coded according to each galaxy's magnification. The black dashed line at log($L_{H\alpha}/L_{UV}$) = 13.4 denotes our completeness limit for the sample. The angled colored space demonstrates the 3σ Hα sensitivity limit of our detector color coded according to magnification. Errors on M_{UV} do NOT include uncertainties on the lens model.

18 galaxies fainter than $M_{UV} = -19$ could have been observed below this line, given their magnifications. This suggests that there are indeed very few galaxies with log($L_{H\alpha}/L_{UV}$) < 13.4 and that our measured increase of log($L_{H\alpha}/L_{UV}$) for faint galaxies is real, and not due to a bias against galaxies with low log($L_{H\alpha}/L_{UV}$). Our final Hα sample after all of these considerations is 23 galaxies.

2.3 Methods

2.3.1 Hα fits

The fits to the Hα line were performed in a manner similar to Gburek et al. (2019) on the 1D extracted MOSFIRE spectra. We briefly review the procedure here. The spectra were fit using an MCMC sampler algorithm *emcee* (Foreman-Mackey et al. 2013). Each of the J,H, and K bands were fit separately and the emission lines were parameterized with a Gaussian and a linear continuum fit. The redshift was taken to be the weighted average of the values obtained between bands with emission lines present. The flux of the Hα line was taken from the Gaussian parameterization.

2.3.2 UV continuum fits

We identified four types of spectra with respect to the Lyα line in our dataset. Adopting the naming conventions of Kornei et al. (2010) we observe Lyα in 'emission', 'absorption', 'combination', and 'noise.' We measure the EWs of these spectra using the conventions of Du et al. (2018) with some variation. For each type of galaxy we set the bounds of numerical integration as follows:

- For emission line galaxies we set the bounds to be where the emission line met the continuum
- For combination and absorption line galaxies we set the region of integration to the space between 1208 Å and 1240 Å. We calculate the continuum level to be the midpoint flux value of a line passing through 1208 Å and 1240 Å, where we take the mean flux between 1206 Å and 1210 Å to be the flux at 1208 Å and the mean flux between 1225

Å and 1255 Å to be the flux at 1240 Å. We use this continuum level for calculating the EW.

- For noise spectra we have no information on the Lyα profile. Therefore, we use boundaries derived by Kornei et al. (2010) at 1199.9 Å and 1228.8 Å rest-frame for the short- and long-wavelength bounds respectively. Where the redshift is determined from the rest-optical emission lines.

In addition, we performed a parameterized fit of the Lyα profile (for emission and combination spectra) and continuum of each spectrum for our galaxy sample to measure the UV spectral slope β. The fitting procedure is performed using a Markov chain Monte Carlo code from pymc3. The wavelength range used for fitting varied based on redshift as the short-wavelength bound was set to just blueward of the Lyα emission line. The long-wavelength bound was set to be at 5450 Å in the observed frame, as the transmission decreases at longer wavelengths due to the dichroic at 5600Å. Typical emission and absorption lines (SiII$\lambda\lambda$1260 Å, OI+SiII$\lambda\lambda$1303 Å, CII$\lambda\lambda$1334 Å, SiIV$\lambda\lambda$1393 Å, CIV$\lambda\lambda$1549 Å, HeII$\lambda\lambda$1640 Å, OIII$\lambda\lambda$1666 Å, CIII$\lambda\lambda$1909 Å, and OIV$\lambda\lambda$1343 Å) were masked when fitting each spectrum. We set the width for these masks to be 800 km s^{-1} except for the CIV$\lambda\lambda$1549 Å line which we set to have an asymmetric width of 1400 km s^{-1} with the blue side of the line extending to -1000 km s^{-1} because of the P-Cygni profile that CIV$\lambda\lambda$1549 Å tends to take. This process was repeated for all galaxies observed. The 'emission' spectra are modelled simultaneously with a power law continuum and a Gaussian emission line to handle correlations between parameters,

$$f_\lambda = A_0 e^{-\frac{(\lambda-\lambda_0)^2}{2\sigma^2}} + B_0(\frac{\lambda}{\lambda_c})^\beta \tag{2.1}$$

For the 'combination' spectra we add in a first order approximation to the Lyα absorption profile,

$$f_\lambda = \begin{cases} A_0 e^{-\frac{(\lambda-\lambda_0)^2}{2\sigma^2}} + a\lambda + b, & \lambda < \lambda_s \\ B_0(\frac{\lambda}{\lambda_c})^\beta, & \lambda > \lambda_s \end{cases} \tag{2.2}$$

Where λ_s is the wavelength where there exists a change in the UV spectral slope likely due to damped Lyα absorption. We fit this region with a linear function to account for the change in the UV spectral slope. The remaining galaxies are parameterized with a power law continuum redward of Lyα (identified either from damped Lyα absorption or from the redshift estimate obtained with Keck/MOSFIRE),

$$f_\lambda = A_0(\frac{\lambda}{\lambda_0})^\beta \tag{2.3}$$

We use an upper limit of FWHM = 4.9 Å rest-frame to obtain upper limits on the flux from the 'absorption' and 'noise' spectra. The value of 4.9 Å is derived from the distribution of 49 FWHMs from the sample for which we have Lyα in emission. 4.9 Å is greater than all but two of 49 (4%) of the FWHMs measured and therefore serves as an upper limit on the FWHM.

2.3.3 Magnification

Thanks to lensing, the signal from faint galaxies is magnified and we are able to extend spectroscopic studies to fainter magnitudes at $z \sim 2$ in just a few hours of Keck/LRIS and Keck/MOSFIRE time (see table 3.1). Our galaxies are observed behind three lensing

clusters. In the X_{LAE} and Hα sub-samples the magnifications span $1.25 \leq \mu \leq 29.12$. The median magnifications are $\langle\mu\rangle_{\rm median} = 7.11$ and $\langle\mu\rangle_{\rm median} = 7.45$ respectively. It is important to properly model the lensing in order to accurately measure the UV luminosity of the galaxies. Alavi et al. (2016) details the lens models used to measure the magnifications of the galaxies behind MACS J0717, MACS J1149, and Abell 1689. The models considered are constrained by the location and redshift of known multiply-imaged sources. We use the models produced by the Clusters As Telescopes (CATS) collaboration[2]. As Alavi et al. (2016) states, we use the models of Limousin et al. (2007), Limousin, M. et al. (2016) and Jauzac et al. (2016) for Abell1689, MACS J0717, and MACS J1149 respectively. These models are derived using `LENSTOOL` [3] (Jullo et al. 2007). The basic assumptions of the model are that the mass ditributions of the clusters is constructed from smooth parameterized large-scale potentials (see Priewe et al. 2017, and reference therein for more details). The uncertainties in the magnification are not considered throughout this work. For the Hubble frontier fields Priewe et al. (2017) show that the systematic uncertainty across lensing models will be on the order of 50% at our magnifications. This is small relative to our "faint" to "bright" delineation which we use for comparisons in M_{UV}. In addition, many of the quantities we consider are relative measures, and since magnification is achromatic the majority of quantities studied in this paper will not be effected by the magnification.

[2] https://archive.stsci.edu/prepds/frontier/lensmodels/

[3] https://projets.lam.fr/projects/lenstool/wiki

2.3.4 SED fits

We fit spectral energy distributions (SEDs) to our Hubble photometry in the near-UV, optical, and near-IR. Before SED-fitting we subtract off contributions from nebular emission lines using our slit-loss corrected spectra. We add an additional 3% flux error to all of our bands to account for systematic errors in our photometry (Alavi et al. 2016). Using the code `FAST`[4] (Kriek et al. 2009), we fit Bruzual & Charlot (2003) stellar population synthesis models to the emission-line subtracted photometry under the following assumptions:

- Constant star formation histories (SFHs)
- A Chabrier (2003) initial mass function (IMF)
- Stellar metallicities of either 0.2 $Z_{\odot}$ or 0.4 $Z_{\odot}$
- A Gordon et al. (SMC, 2003) dust attenuation curve

Galaxy redshifts are set by the fit curves to the rest-optical spectroscopy. M_{UV} is calculated from the closest filter to the rest-frame 1700 Å that doesn't include Lyα, and uncertainties on M_{UV} are statistical.

2.3.5 Dust Correction

In our analysis of the Hα sample we need to correct the Hα line and the UV continuum at 1700 Å for dust attenuation. We use the SMC curve of Gordon et al. (2003) and A_V estimates from our SED fitting to estimate the attenuation of the UV continuum. We make use of the SMC attenuation law for the UV continuum because it has been shown

[4] `https://w.astro.berkeley.edu/~mariska/FAST.html`

to be more accurate for high-redshft and low-metallicity galaxies than the Cardelli et al. (1989) curve (e.g. Reddy et al. 2022). The correction for Hα is estimated by measurement of the Balmer decrement (assuming Case-B recombination). However, many of our galaxies have Balmer lines that are either too faint or obscured by sky emission and we are unable to directly measure the Balmer decrement of each galaxy. We split our Hα sample into bright ($M_{UV} < -19$) and faint ($M_{UV} > -19$) sub-samples for which we estimate A_V. For the faint sub-sample we normalize the spectra by Hα and perform a median stack of the galaxies. We use a Cardelli et al. (1989) curve and measure $\langle A_V \rangle = 0.54$ and apply this to all of our dwarf galaxies. Most of our reported results will be about the dwarf galaxies for which we use this average attenuation value. We recognize that there will be significant scatter around this value. Nonetheless, the correction is small, a factor of 1.5 for the Hα luminosity, and does not affect the average trends reported in this paper. For our more massive galaxies we measure A_V for three of the galaxies ($A_V = 1.14,\ 0.88,$ and 0.80). We then use the mean ($\langle A_V \rangle = 0.94$) on the remaining two galaxies for which we did not have H_β $S/N > 5$ and therefore could not reliably calculate the dust correction.

2.4 Results

As explained above, our larger X_{LAE} sample is used to measure the EW distribution and the smaller Hα sub-sample is used to measure the escape fraction. We compare our two samples in order to see if the two are similar and therefore both can be used to determine properties of dwarf galaxies at this redshift. We find that the median EWs agree within errors on the median as shown in figure 2.4. We calculate the uncertainty on the

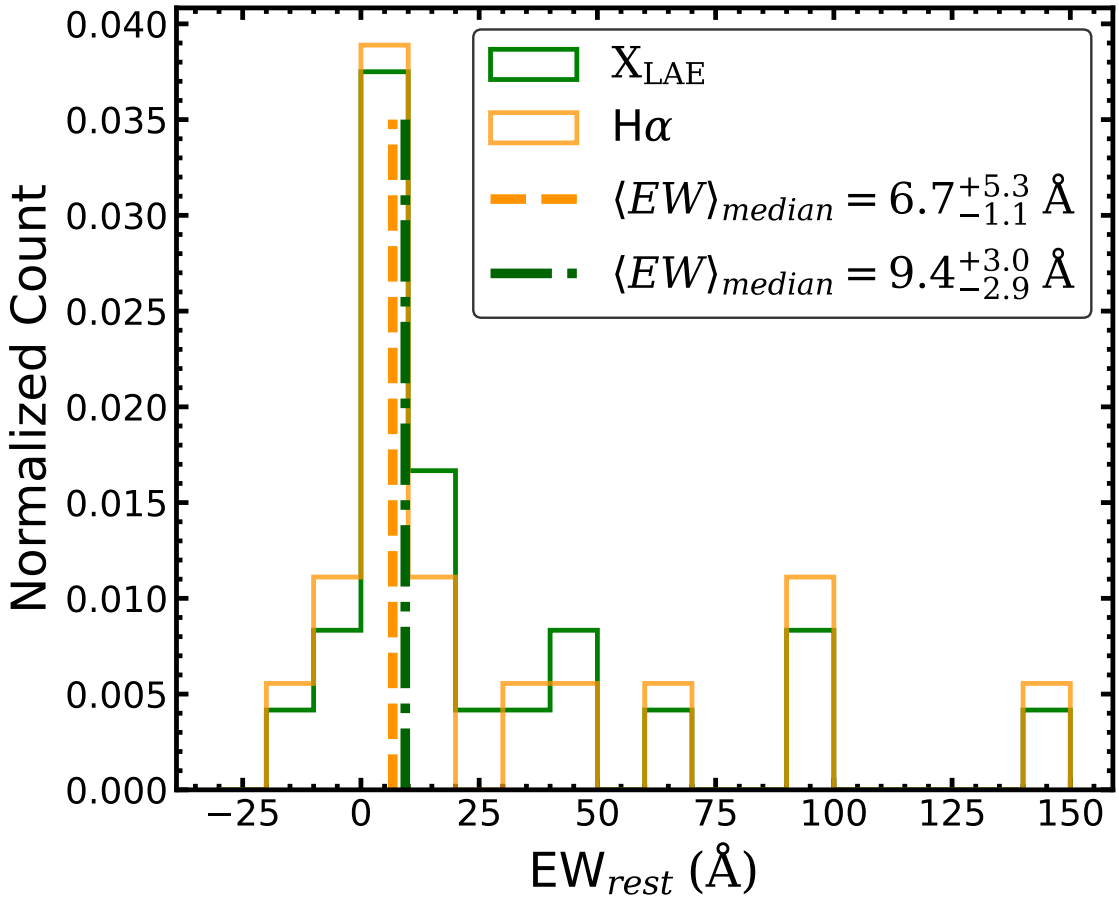

Figure 2.4: The green (orange) histogram is a normalized distribution of rest-frame EWs of our X_{LAE} (Hα) sample. The colored dashed vertical lines show the median EW of $9.4^{+3.0}_{-2.9}$ ($6.7^{+5.3}_{-1.1}$) for the X_{LAE} (Hα) sample. The Lyα EW distributions of both samples are consistent.

median for each sample by randomly selecting galaxies within the given sample with replacement and recalculating the median from this new sample. We perform this operation 10,000 times and define the errors as the 16th and 84th percentiles of the distribution of the median. The difference in mean redshift is small ($\langle z_{Ly\alpha}\rangle = 2.28$ and $\langle z_{H\alpha}\rangle = 2.23$). Since the distributions are similar we take the Hα sample to be representative of trends in the X_{LAE} sample as well.

2.4.1 Lyα EW distribution

We wish to investigate trends in the EW distribution with UV luminosity. Therefore we wish to compare with a sample of higher luminosity galaxies at similar redshifts where possible. Therefore, we compare our EW distribution with that of the higher luminosity ($M_{UV} \sim -20$) sample of Du et al. (2021) as shown in Figure 2.5. We find that our sample is skewed towards larger Lyα EWs. The median EW for the Du et al. (2021) sample is $-6.0^{+1.9}_{-1.1}$ Å and the median for our sample is $9.4^{+3.0}_{-2.9}$ Å. The two distributions differ by $\sim 4\sigma$ showing that they are statistically different. We calculate the uncertainty for the Du et al. (2021) median in the same manner used for each of our sub-samples.

The cutoff for defining a LAE in the literature varies significantly depending on the study (Stark et al. 2010, 2011; Caruana et al. 2018; Kusakabe et al. 2020, etc.). However, the most common cuts are EW $>$ 20 Å, EW $>$ 25 Å, and EW $>$ 55 Å, so we will use these cuts as well. For these three cutoffs we measure $X_{LAE} = 33^{+17}_{-12}\%$ (8/24), $33^{+17}_{-12}\%$ (8/24), and $17^{+13}_{-8}\%$ (4/24), respectively. We assume a Poisson distribution to estimate uncertainties on X_{LAE}. X_{LAE} measurements of brighter galaxies are $\sim 11\%$ for EW $>$ 20 Å at $z \sim 2$ (12% from Reddy et al. (2008), 11.1% from Hathi et al. (2016), and 10.7% from Du et al. (2021)). For brighter galaxies with EW $>$ 25 Å and EW $>$ 55 Å at $z \sim 2$ $X_{LAE} = 10\%$ and 4% respectively (Cassata et al. 2015). These data suggest that galaxies fainter than $M_{UV} = -19$ have greater numbers of LAEs in their population. We explore this in more detail in section 2.5.3.

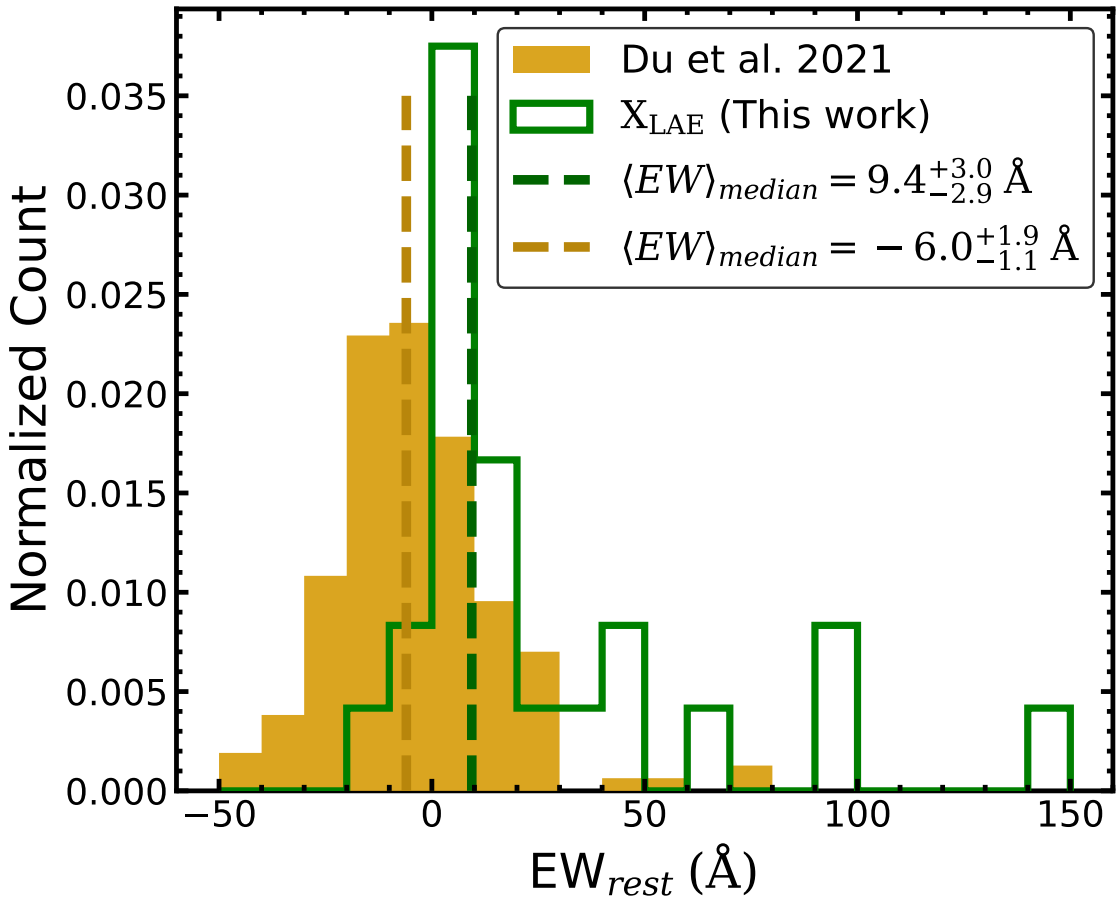

Figure 2.5: The green histogram is a normalized distribution of rest-frame EWs of our X_{LAE} sample. The gold histogram is a normalized distribution of rest-frame EWs of the brighter sample from Du et al. (2021). The vertical dashed lines of corresponding color show the median Lyα EWs of each sample. the median EWs of the green and gold histograms are $\langle EW \rangle_{median} = 9.4^{+3.0}_{-2.9}$ Å and $\langle EW \rangle_{median} = -6.0^{+1.9}_{-1.1}$ Å respectively.

2.4.2 Escape Fraction

In our Hα sample for which we are able to measure the escape fraction of Lyα photons we assume a Case-B scenario for which the gas is taken to be optically thick for the Lyman series. The ratio of the flux of Lyα to the flux of Hα under this assumption can vary depending on the temperature and electron density of the galaxy. We choose to use a ratio of 8.7 which is common in the literature (e.g. Matthee et al. 2016). We then measure the escape fractions of individual galaxies as

$$f_{\rm esc} = \frac{F_{\rm Ly\alpha}}{8.7\ F_{\rm H\alpha,cor}} \tag{2.4}$$

where $\rm F_{Ly\alpha}$ is the Lyα flux and $\rm F_{H\alpha,cor}$ is the dust corrected Hα flux. The mean of the individual $f_{\rm esc}$ measurements is $4.3^{+1.6}_{-1.1}\%$. We estimate the uncertainty in the mean via a bootstrap method. We perturb each measurement of the sample according to a Gaussian distribution with standard deviation set by the uncertainty of the measurement and then resample by randomly selecting with replacement from our perturbed sample and then calculating the mean of the escape fractions. This process is performed 100,000 times. We then take the 16th and 84th percentiles of the 100,000 iterations to be the uncertainty on the mean escape fraction.

However, this value may not be representative of the actual number of Lyα photons escaping into the intergalactic medium. The intrinsic luminosity of galaxies varies greatly and may correlate with Lyα escape fraction. Thus, the mean escape fraction may be different from the net output from all galaxies, which we refer to as the *volumetric* escape fraction. To calculate the volumetric escape fraction, we first need to determine the galaxies' intrinsic luminosity and, thus, de-magnify each of our galaxies. We then replace the fluxes in Eq.

2.4 with the sum of the respective luminosities. We measure a volumetric escape fraction of $4.6^{+2.0}_{-1.4}\%$. We estimate the uncertainty in a similar manner to the individual escape fraction estimate. We perturb each measurement of the sample according to a Gaussian distribution with standard deviation set by the uncertainty of the measurements, resample, and then calculate the volumetric escape fraction. We take the 16th and 84th percentiles of the 100,000 iterations to be the uncertainty on the volumetric escape fraction. This method includes contributions from uncertainties in the dust correction. This value agrees well with what is found in the literature ($5.3\% \pm 3.8\%$ at $M_{UV} \sim -19$ in Hayes et al. (2010), $4.4^{+2.1}_{-1.2}\%$ at $M_{UV} \sim -19.5$ in Ciardullo et al. (2014), $5.1\% \pm 0.2\%$ at $M_{UV} \sim -19.7$ in Sobral et al. (2017), and $5.8^{+0.7}_{-0.5}\%$ at $M_{UV} \sim -19.5$ in Weiss et al. (2021)).

By the use of gravitational lensing we were able to directly measure a UV selected sample of dwarf galaxies at $z = 2$. We are able to probe fainter Hα and Lyα luminosities and have a greater sample of joint detections of Hα and Lyα emitters than what was observed in Hayes et al. (2010).

2.4.3 Observed Lyα EW

We investigate which galaxies are emitting most of the Lyα luminosity. Figure 2.6 shows that about 60% of the integrated Lyα luminosity density comes from galaxies with $EW_{Ly\alpha} > 20$ Å. This suggests that LAEs are contributing a large fraction of the Lyα photons. This cumulative distribution can also be calculated from narrow-band surveys for Lyα. However, those surveys can not determine the amount of total emissions from low

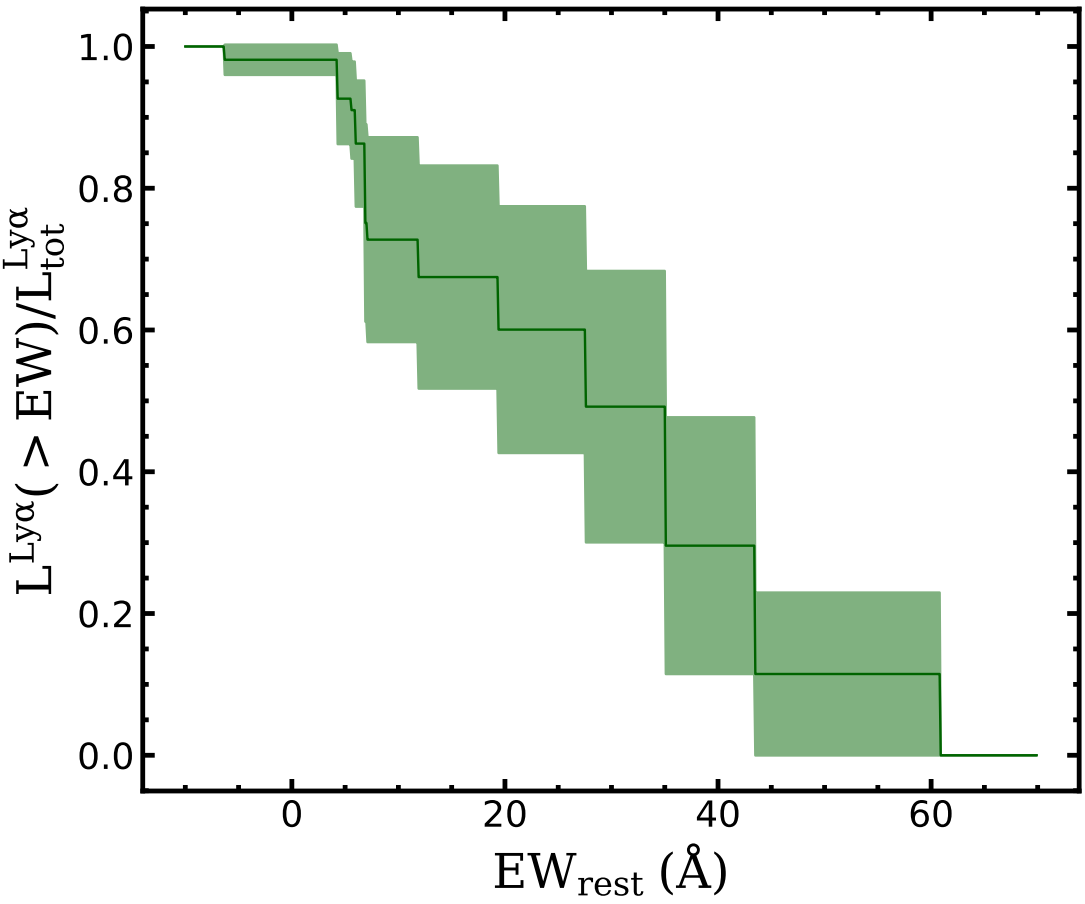

Figure 2.6: The integrated Lyα luminosity density as a function of EW. The uncertainty is given by the shaded green regions. We find that about 60% of the integrated luminosity density comes from galaxies with $EW_{Ly\alpha} > 20$ Å

EW galaxies. Here we show that $\sim 10-20\%$ of the Lyα luminosity density comes from galaxies with $\mathrm{EW}_{\mathrm{Ly}\alpha} < 5$Å.

2.5 Discussion

Here we seek to understand the origins of the observed EW distribution. Is the spread in observed EW primarily due to varying escape fractions, or are variations in stellar populations (in particular, starburst age), creating a large scatter in *intrinsic* EWs as well.

2.5.1 Intrinsic Lyα EW

To investigate influences from the stellar populations we make use of the intrinsic Lyα EW

$$\mathrm{EW}_{\mathrm{int}} = \frac{8.7\mathrm{L}_{\mathrm{H}\alpha,\mathrm{cor}}}{\mathrm{L}_{\lambda,1216,\mathrm{cor}}} \tag{2.5}$$

where $\mathrm{L}_{\mathrm{H}\alpha,\mathrm{cor}}$ is the dust-corrected and de-magnified Hα luminosity, and $\mathrm{L}_{\lambda,1216,\mathrm{cor}}$ is the dust corrected and de-magnified UV luminosity density extrapolated to 1216 Å. Figure 2.7 shows the intrinsic EW as a function of absolute UV magnitude. We note that since we make use of $\mathrm{A_V}$ values from SED fitting to correct the UV luminosity we must remove 5 galaxies for which we do not have sufficient photometric coverage to perform SED fits from all analysis regarding intrinsic EWs.

We compare our measured $\mathrm{EW}_{\mathrm{int}}$ values to those of more massive galaxies at the same redshift. We convert the ionizing photon production efficiency (ξ_{ion}) of Shivaei et al. (2018) to $\mathrm{EW}_{\mathrm{int}}$ by converting ξ_{ion} to $\mathrm{L}_{\mathrm{Ly}\alpha}/\mathrm{L}_{\mathrm{UV}}$. In Shivaei et al. (2018) they calculate ξ_{ion} from weighted mean stacks of their galaxies in bins of absolute UV magnitude. They are

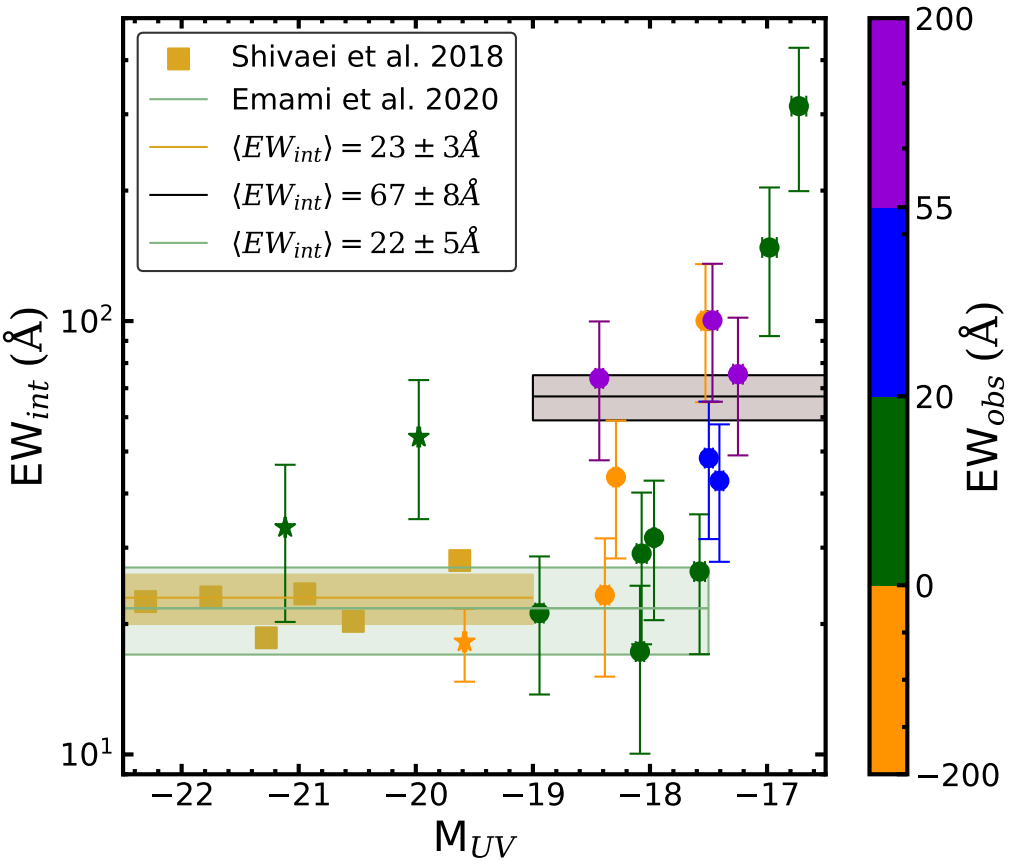

Figure 2.7: The *intrinsic* equivalent width as a function of absolute UV magnitude (M_{UV}). Points are color coded according to the *observed* equivalent width (see color bar on the right) with blue and purple points representing galaxies observed as LAEs. The square gold points are average values of higher luminosity galaxies and are derived from the ξ_{ion} measurements of Shivaei et al. (2018). Galaxies brighter than -19 in absolute UV magnitude are plotted with a star, while fainter galaxies are plotted with filled circles. We show the mean intrinsic EW of Shivaei et al. (2018) and uncertainty in the mean with a gold shaded region, and we show the mean intrinsic EW and uncertainty in the mean of our dwarf galaxy sample in brown. We also show the mean intrinsic EW and uncertainty in the mean of Emami et al. (2020), which includes some of the same galaxies, with a green shaded region. Five galaxies did not have sufficient photometric coverage to perform SED fitting to obtain A_V values to correct the UV luminosity and are removed from any intrinsic EW analysis.

shown as gold squares in figure 2.7. Shivaei et al. (2018) show a mean $\log(\xi_{\rm ion}) = 25.36 \pm 0.06$ for the SMC curve. This corresponds to an intrinsic EW of $23 \text{Å} \pm 3$ Å. Emami et al. (2020) have $\xi_{\rm ion} = 25.22 \pm 0.10$ which corresponds to an intrinsic EW of 22 ± 5 Å for a similar sample. For our faint galaxies our mean intrinsic EW is 67 ± 8 Å. Therefore, we see a significant increase in the mean intrinsic EW for fainter galaxies. The faintest galaxies in our sample may be skewing the sample toward higher $\text{EW}_{\rm int}$, but if we remove the two faintest galaxies we still get an elevated mean intrinsic EW of 46 ± 5 Å. We also show in figure 2.7 the observed EWs via the colorbar where blue and purple points indicate LAEs. From the plot we observe large intrinsic EWs ($\text{EW}_{\rm int} > 40$ Å) facilitate observation of LAEs, but are not a guarantee that a galaxy will be observed as a LAE. This implies that the ionizing output of the stellar population in galaxies has significant bearing on whether a galaxy is observed to be a LAE. However, it is clear that the stellar population alone cannot account for the observability of LAEs.

2.5.2 Escape Fraction $f_{\rm esc}$

The other factor driving the observed distribution in Lyα EWs is whether the photons actually escape from the galaxy. With our MOSFIRE spectra we are able to measure this value directly. For our absorption galaxies in the Hα sample we set $f_{\rm esc} = 0$. We show the escape fraction as a function of absolute UV magnitude in figure 2.8.

We see large scatter in the escape fraction at faint absolute UV magnitudes. It is also the case that no escape fraction less than $\sim 5\%$ is observed as a Lyα emitter. Therefore, it is clear that the escape of ionizing photons plays a crucial role in the observed

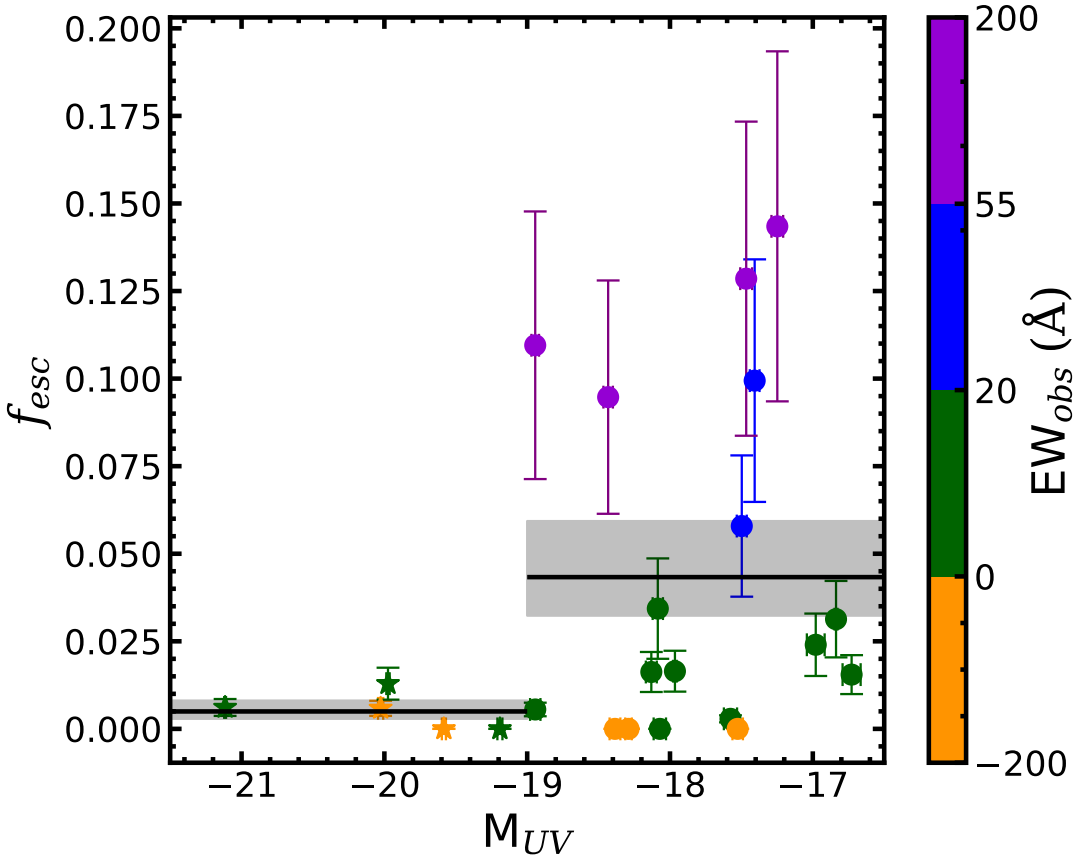

Figure 2.8: The Lyα escape fraction as a function of absolute UV magnitude (M_{UV}). The color coding and markers are the same as in figure 2.7. The mean escape fraction of the dwarf galaxies ($4.3^{+1.6}_{-1.1}\%$) and the more massive galaxies ($0.5^{+0.3}_{-0.2}\%$) are displayed with shaded black regions denoting the propagated uncertainty in the individual galaxies. However, the bright galaxy sample has only 5 galaxies and is therefore uncertain.

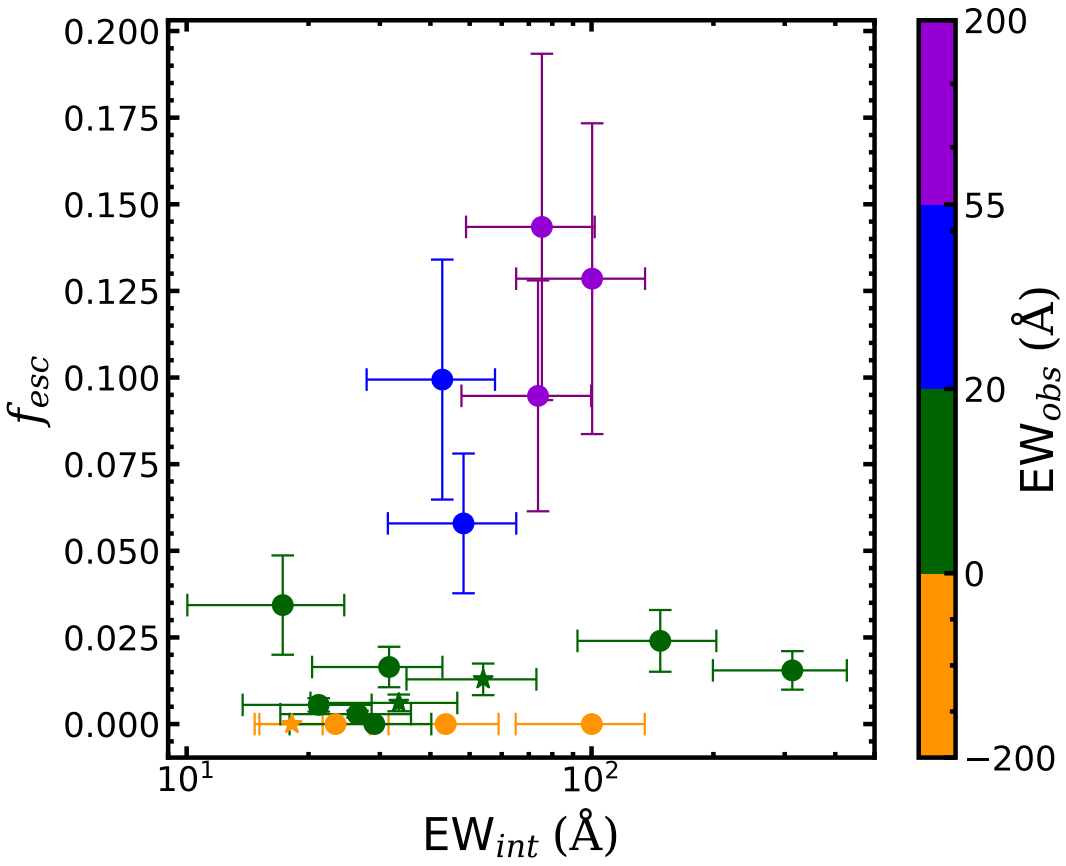

Figure 2.9: The Lyα escape fraction as a function of *intrinsic* equivalent width. The color coding and markers are the same as in figure 2.7. Galaxies with no Lyα in emission are set to $f_{\rm esc} = 0$. We observe that only galaxies with intrinsic equivalent widths greater than 40 Å have escape fractions greater than 5%.

EW distribution and $X_{\rm LAE}$. To determine if the escape fraction and $EW_{\rm int}$ are correlated, we plot them against each other in figure 2.9.

We see that 5/9 of the galaxies with high intrinsic EWs ($\geq$ 40 Å) have large escape fractions ($f_{\rm esc} > 5\%$). No galaxy (0/8) with $EW_{\rm int} < 40$ Å has an escape fraction larger than 5%. We can set two conditions for LAEs; LAEs have escape fractions greater than 5% and intrinsic EWs greater than 40 Å. We caution that our sample size is small, so this

result could be made more robust by increasing the sample size. In order to understand this a little deeper we can look at possible drivers of the escape fraction.

Lyα can be heavily attenuated by dust. However, in our sample we have shown that our galaxies are typically not very dusty. Nevertheless we check to see if there is any relation between the dust attenuation estimated from SED fits and the escape fraction. Figure 2.10 shows the escape fraction as a function of A_V. We observe an anti-correlation between f_{esc} and A_V. However, nearly all of our galaxies have $A_V \leq 0.2$. With little variance in dust content we aren't able to test this robustly. Nevertheless, we don't observe escape fractions greater than 5% for $A_V \geq 0.2$. To test the anti-correlation we perform an MCMC fit for a linear model and find the slope to be -0.015 ± 0.004. This establishes the anti-correlation at greater than 3σ. We also note that the two highest intrinsic EW objects also exhibit dust content similar to our LAEs. This suggests that it is primarily attenuation by neutral hydrogen dictating the escape of Lyα photons in dwarf galaxies. Cassata et al. (2015) show that there is larger variance in f_{esc} at a given reddening value (see their figure 6) which is consistent with our results. Our highest dust bins have few data points and might not be representative. Our two lowest dust content bins may suggest a constant average escape fraction as a function of A_V which appears to be consistent with the lowest redshift bins of Matthee et al. (2016) with $3''$ apertures. This is in slight contrast to the measurements of Weiss et al. (2021) who show a steep increase in f_{esc} with decreasing reddening. However, the sample of Weiss et al. (2021) may be biased towards LAEs, particularly at the lowest mass/dust values ($\log(M^\star/M_\odot) < 9$), which is the regime of our study, since they are selecting on [OIII]5007 emission (Erb et al. 2016). That they are

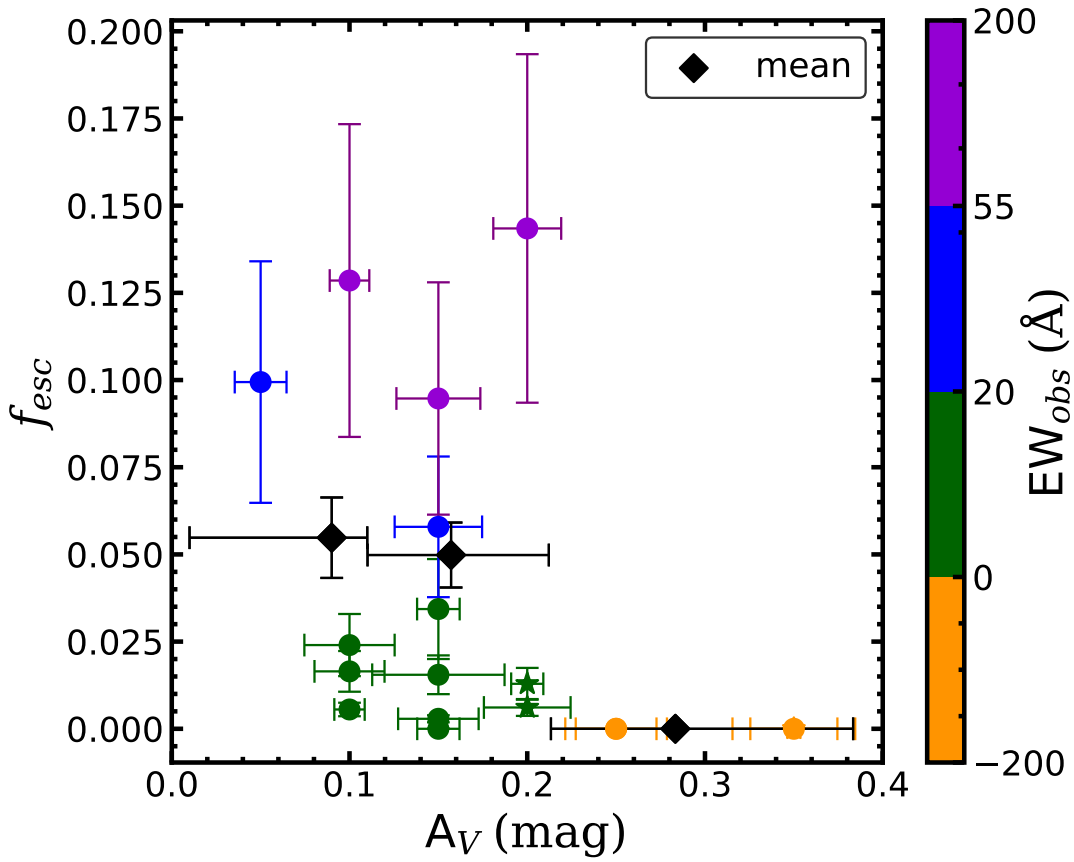

Figure 2.10: The Lyα escape fraction as a function of dust attenuation. The color coding and markers are the same as in figure 2.7. Black diamonds show the mean escape fraction in three bins of A_V. The horizontal error bars denote the sizes of the bins and the vertical error bars denote the uncertainty in the mean. A_V is here derived from SED fitting of Hubble photometry and is in discreet steps.

biased at the low mass end is supported by the left panel of their figure 4 which indicates that their typical galaxy at low mass is a LAE.

The slope of the UV continuum can also be used as an indicator of dust and so we look at possible correlations with UV slope as well. This is shown in figure 2.11. Here we see a mild dependence in that the scatter of escape fractions increases for $\beta < -0.5$. Together, figures 2.10 and 2.11 suggest that there is a slight anti-correlation between dust

and $f_{\rm esc}$ for faint galaxies. We again test the anti-correlation using an MCMC routine and a linear model and find a slope of -0.0003 ± 0.0011. Therefore, our data are consistent with there being no correlation between f_{esc} and UV spectral slope. We suggest that the trend in the mean is marginal for our small data set. Matthee et al. (2016) show a change in the slope of the trend between $f_{\rm esc}$ and β which we do not see for our dwarf galaxies. However, we lack sufficient numbers of $\beta > 0$ galaxies to make any definitive statements regarding this change. We are inconsistent with Matthee et al. (2016) regarding the decrease in $f_{\rm esc}$ with β out to $\beta = 0$. This may be due to our small sample size.

2.5.3 Trends in $X_{\rm LAE}$

The decrement in $X_{\rm LAE}$ from the expected $X_{\rm LAE}$ at high redshift is often used to infer the IGM neutral fraction (Stark et al. 2010, 2011, e.g.). However, in order to investigate the number of faint galaxies that contribute to reionization it is helpful to establish trends in $X_{\rm LAE}$ with $M_{\rm UV}$ at lower redshifts where Lyα is observable. To this end we compare with the VUDS sample (Le Fèvre et al. 2015; Hathi et al. 2016; Cassata et al. 2015) at higher UV luminosities. For this analysis we choose $EW_{\rm Ly\alpha} > 20$ Å as our definition for a LAE. Figure 2.12 shows the VUDS data set in bins of $M_{\rm UV}$ along with our data set. The uncertainty on the VUDS bins were calculated by re-sampling the distribution within each $M_{\rm UV}$ bin. The same number of galaxies within the bin were randomly selected with replacement and then the fraction of LAEs was calculated. This procedure was repeated 10,000 times on each bin and the standard deviation of $X_{\rm LAE}$ values from this procedure was taken to be the 1-σ uncertainty on the VUDS bins. For our $X_{\rm LAE}$ value we assume Poisson statistics (due to

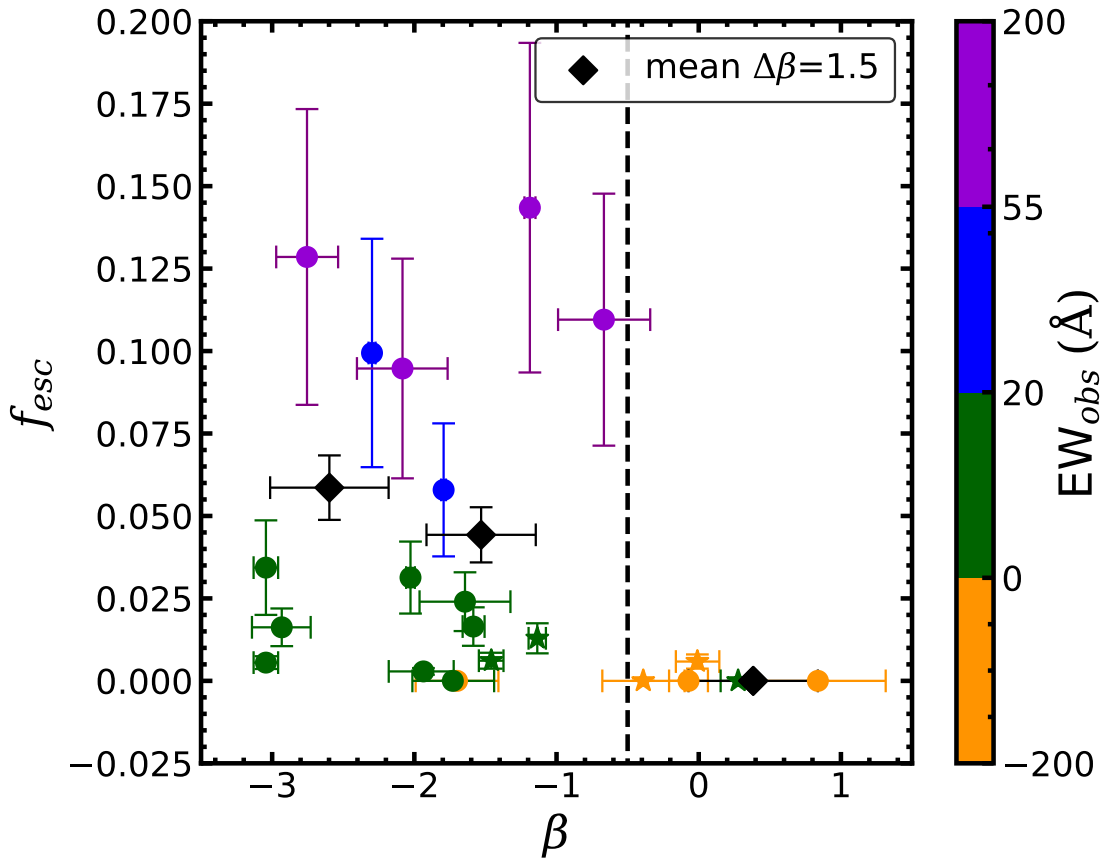

Figure 2.11: The Lyα escape fraction as a function of UV spectral slope (β). The color coding and markers are the same as in figure 2.7. The black dashed vertical line is set as a limit for LAEs. All LAEs have slopes bluer than -0.5. There is large variance in beta for similar $f_{\rm esc}$, perhaps suggesting bursty star-formation. The black diamonds are mean values of the escape fraction in bins of $\Delta\beta = 1.5$. The error bars are calculated by propagating the statistical uncertainty of each datum. One object was excluded due to highly uncertain β from low S/N continuum.

the small number of galaxies in our data set) to estimate the uncertainty. We find no trend in the VUDS data for brighter M_{UV}, so we fit a constant line to the VUDS data set. We assume a bimodal probability distribution for fitting X_{LAE} in the VUDS data of the form,

$$p(data|X_{LAE}) \sim X_{LAE}^{L}(1 - X_{LAE})^{N-L} \tag{2.6}$$

where N is the total number of galaxies and L is the number of LAEs. This gives a most likely value for the fit to the VUDS data of $X_{LAE} = 0.101 \pm 0.012$. This is $\sim 2\sigma$ from our result of $X_{LAE} = 0.33^{+0.17}_{-0.12}$. More data at $M_{UV} \sim -19$ between the VUDS faintest M_{UV} and our sample is necessary to determine any trend in X_{LAE} with M_{UV}.

We also investigate trends in redshift using the VUDS data set as shown in figure 2.13. We fit each redshift bin with a constant value, according to the same method used for the z$\sim$2 sample, since we again see no trend with M_{UV} at any redshift. There is a clear trend towards larger X_{LAE} with redshift in agreement with other works in the literature (e.g. Stark et al. 2011; De La Vieuville et al. 2020; Kusakabe et al. 2020). The X_{LAE} values of low luminosity galaxies at $z \sim 2$ in our sample are consistent with more massive galaxies at $z \geq 3$.

2.6 Summary

In this paper we have investigated the distribution of Lyα EWs for dwarf galaxies at $z \sim 2$. We selected (via UV continuum) magnified galaxies behind lensing clusters, allowing us to obtain rest-UV spectroscopy for some of the faintest galaxies ($M_{UV} < -17$, $\langle M^{\star} \rangle_{median} = 10^{8.4}$ $M_{\odot}$) observed at $z \sim 2$. We reduce our sample to avoid issues with

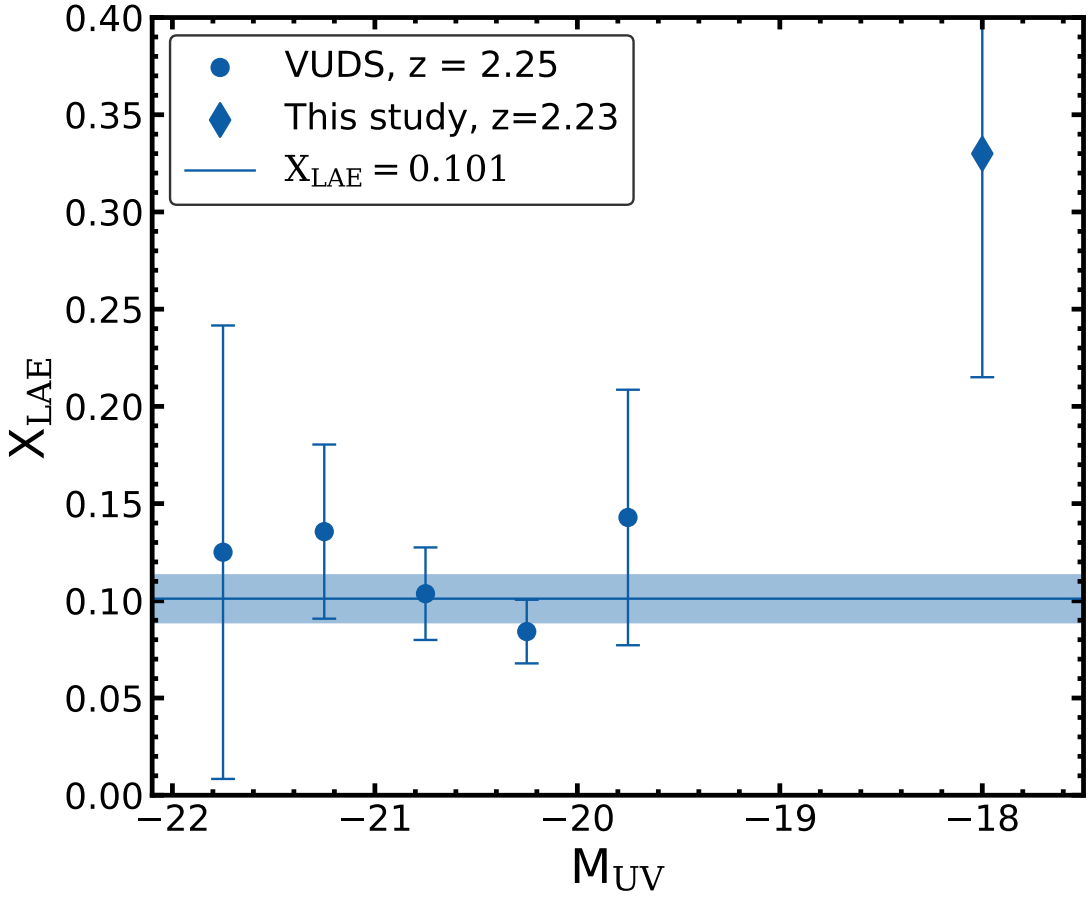

Figure 2.12: The Lyα emitter fraction, X_{LAE}, as a function of M_{UV}. Our data set is represented by a blue diamond and the VUDS dataset by blue circles. We show a constant fit line, along with uncertainties in shaded blue, to the VUDS data at $X_{LAE} = 0.101 \pm 0.012$ as there is no trend in the brighter M_{UV} sample.

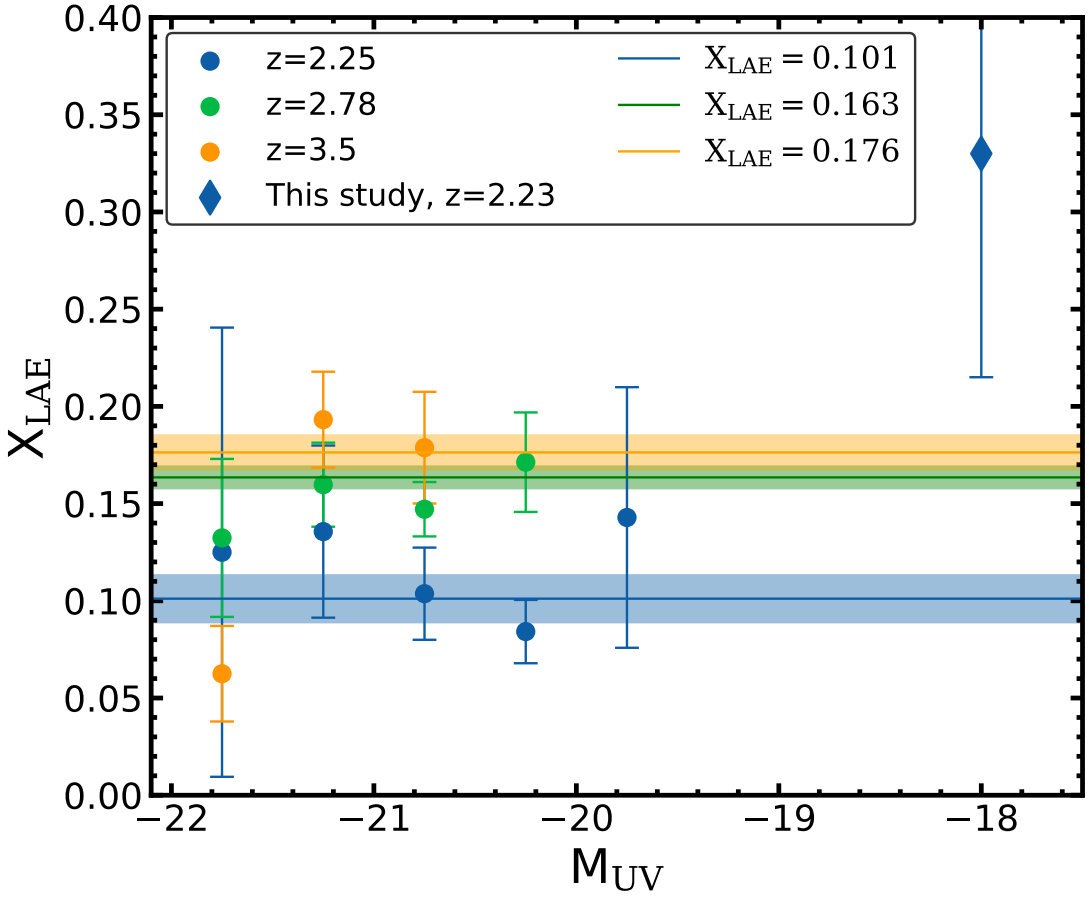

Figure 2.13: The Lyα emitter fraction, X_{LAE}, as a function of absolute UV magnitude and redshift. The lines and shaded regions of corresponding color to the data points are the constant fit curves to the data at each redshift. There are no trends in M_{UV} at any redshift in the VUDS data.

differential magnification, large slit loss uncertainties, incompleteness due to faint Hα, and the observability of Lyα and Hα within the bands of Keck/LRIS and Keck/MOSFIRE. We then analyze the EW distribution of the sample and draw the following conclusions:

- The observed $EW_{Ly\alpha}$ distribution of low UV luminosity galaxies is skewed towards larger $EW_{Ly\alpha}$ than higher luminosity galaxies such as those in the KBSS sample of Du et al. (2021). Our sample shows a median $EW_{Ly\alpha}$ of $9.4^{+3.0}_{-2.9}$ Å whereas the sample of Du et al. (2021) shows a median $EW_{Ly\alpha}$ of $-6.0^{+1.9}_{-1.1}$ Å.

- The fraction of galaxies that are Lyα emitters, X_{LAE}, is $33^{+17}_{-12}\%$, $33^{+17}_{-12}\%$, and $17^{+13}_{-8}\%$ for $EW_{Ly\alpha} > 20$ Å, $EW_{Ly\alpha} > 25$ Å, and $EW_{Ly\alpha} > 55$ Å respectively. These values are greater than X_{LAE} ($EW_{Ly\alpha} > 20$ Å) in higher luminosity samples such as Reddy et al. (12%, 2008), Hathi et al. (11%, 2016), and Du et al. (11%, 2021).

- We investigate possible trends in X_{LAE} with M_{UV} and redshift using the VUDS data set (Le Fèvre et al. 2015; Hathi et al. 2016; Cassata et al. 2015). We find no trend with M_{UV} between $-22 \leq M_{UV} \leq -19.5$, but find our X_{LAE} at $M_{UV} \sim -18$ to be about a factor of 3 greater at $\sim 2\sigma$ significance. There is a trend towards larger X_{LAE} with redshift in the VUDS data. Further investigation of dwarf galaxies at higher redshift could show increased X_{LAE} relative to higher mass galaxies as well.

- We find that the total integrated Lyα luminosity is 60% for galaxies with $EW_{Ly\alpha} > 20$ Å, suggesting that LAEs contribute a large fraction of the Lyα photons. We also find that $\sim 10 - 20\%$ of the integrated luminosity comes from galaxies with $EW_{Ly\alpha} < 5$ Å.

- We estimate the intrinsic Lyα EW of galaxies, and show an increase in the mean $\mathrm{EW_{int}}$ for faint galaxies ($\langle \mathrm{EW_{int}} \rangle = 67 \pm 8$ Å) compared to the brighter sample of Shivaei et al. (2018, $\langle \mathrm{EW_{int}} \rangle = 23 \pm 3$ Å) and the intermediate luminosity sample of Emami et al. (2020, $\langle \mathrm{EW_{int}} \rangle = 22 \pm 5$ Å). This suggests that younger ages and/or lower metallicities of the stellar populations of dwarf galaxies are increasing the intrinsic EW and contributing to the larger $\mathrm{X_{LAE}}$.

- We investigate the escape fraction of Lyα photons to further understand what is driving the EW distribution. We observe a marginal increase in the mean escape fraction with absolute UV magnitude. We also observe that only galaxies with $\mathrm{EW_{int}} > 40$ Å have $f_{\mathrm{esc}} > 5\%$. This suggests that only galaxies with higher $\mathrm{EW_{int}}$ will be classified as LAEs, not just because of their higher $\mathrm{EW_{int}}$, but also because only those galaxies have large escape fractions.

- We find an anti-correlation between f_{esc} and $\mathrm{A_V}$. This implies that low dust-content facilitates the escape of Lyα photons. However, we have some evidence that for low values of $\mathrm{A_V}$, where scatter in f_{esc} is large, that it is primarily attenuation by neutral hydrogen dictating the escape of Lyα photons.

- We observe a global *volumetric* escape fraction of $f_{\mathrm{esc}} = 4.6^{+2.0}_{-1.4}\%$ in our sample, in good agreement with values inferred for other faint UV luminosity samples in the literature (e.g. Hayes et al. 2010; Weiss et al. 2021, etc.).

We were able to disentangle to some extent two primary drivers of the Lyα EW distribution, namely the ionizing sources (via the intrinsic EW), and the ISM gas/dust content (via the escape fraction and its dependencies). This sample can serve as a baseline

with which to compare higher redshift and higher mass samples. Larger sample sizes of dwarf galaxies would serve to solidify some of the results of this work.

Acknowledgments

This research made use of `PypeIt`[5], a Python package for semi-automated reduction of astronomical slit-based spectroscopy (Prochaska et al. 2020; Prochaska et al. 2020). Some of the data presented herein were obtained at the W. M. Keck Observatory, which is operated as a scientific partnership among the California Institute of Technology, the University of California and the National Aeronautics and Space Administration. The Observatory was made possible by the generous financial support of the W. M. Keck Foundation.

The authors wish to recognize and acknowledge the very significant cultural role and reverence that the summit of Maunakea has always had within the indigenous Hawaiian community. We are most fortunate to have the opportunity to conduct observations from this mountain.

Based on observations made with the NASA/ESA *Hubble Space Telescope*, obtained from the Data Archive at the Space Telescope Science Institute, which is operated by the Association of Universities for Research in Astronomy, Inc., under NASA contract NAS5-26555. These observations are associated with programs #9289, #11710, #11802, #12201, #12931, #13389, #14209.

[5] https://pypeit.readthedocs.io/en/latest/

Data Availability

This paper is based on public data from the Hubble Space Telescope as well as from programs 12201, 12931, 13389, 14209. Spectroscopic data from our survey with the Keck Observatory. These data are available upon request from Christopher Snapp-Kolas or Dr. Brian Siana.

Chapter 3

Paper II: The Rest-UV Spectral Properties of Dwarf Galaxies at $z \sim 2$[1]

Abstract Rest-UV spectroscopy can constrain properties of the stellar populations, outflows, covering fractions, and can indirectly constrain the Lyman continuum escape fraction of galaxies. Many studies have looked at the rest-UV spectroscopy of more massive star forming galaxies and in low-mass galaxies selected via strong nebular line emission or via Lyα emission. However, studies of rest-UV spectroscopy have yet to be done on an unbiased sample at low mass. We present a stacked rest-UV spectrum of a complete sample of dwarf galaxies ($\langle \log(M^*/M_\odot) \rangle_{\rm median} = 8.2$) at $z \sim 2$. The rest-UV Keck/LRIS spectroscopy is

[1]This chapter contains a draft of an article that has been submitted for publication by the Monthly Notices of the Royal Astronomical Society written by C. Snapp-Kolas, B. Siana, T. Gburek, A. Alavi, N. Emami, J. Richard, D.P. Stark, C. Scarlata

complemented by rest-optical Keck/MOSFIRE spectroscopy and Hubble photometry. We find generally larger Lyα equivalent widths ($EW_{Ly\alpha}$ = 10.3 Å) when compared with higher mass ($\langle \log(M^*/M_\odot) \rangle_{median}$ = 10.3) composites from KBSS ($EW_{Ly\alpha}$ = −5 Å). The average low- and high-ionization absorption line EWs (EW_{LIS} and EW_{HIS}, respectively) are weaker by about a factor of two (EW_{LIS}=-0.95 Å, EW_{HIS} =-0.66 Å) in dwarf galaxies than in higher mass galaxies (EW_{LIS}=-2.04 Å, EW_{HIS} =-1.42 Å). These results imply that the escape fraction of ionizing radiation is larger in dwarf galaxies compared to their more massive counterparts at fixed redshift.

3.1 Introduction

The evolution of galaxies over cosmic time is heavily dependent on the cycle of baryons in the intersteller and circumgalactic media (ISM and CGM, respectively). The motion and distribution of gas, dust, and metals in the ISM and CGM dictate the star-formation efficiency and ionizing escape fraction of galaxies. The rest-UV spectra of galaxies can be used to constrain the motion and distribution of gas, dust, and metals. This has been well studied in high-mass ($\log(M^*/M_\odot) > 9$) galaxies at high redshift (e.g. Shapley et al. 2003; Du et al. 2018; Weldon et al. 2022). However, there is yet to be a systematic study of the rest-UV spectra of a complete sample of low-mass galaxies at high redshift.

The rest-UV spectra of galaxies contain complex and informative emission and absorption line profiles. Some of the earliest uses of rest-UV spectroscopy for high redshift galaxies confirmed the redshifts of photometric dropout samples (e.g. Steidel et al. 1996; Lowenthal et al. 1997). More recently properties of the stellar populations and the gas in the

interstellar medium (ISM) have been inferred from the profiles and line depths/heights of the emission and absorption lines present in the rest-UV spectra. In particular, the low- and high-ionization (LIS and HIS respectively) absorption lines can serve to trace the neutral and ionized components of the ISM respectively (e.g. Hashimoto et al. 2013; Du et al. 2018, 2021; Saldana-Lopez et al. 2022). Complementary photometry can serve to correlate the measurements of the lines with galaxy physical properties such as UV luminosity and mass (e.g. Shapley et al. 2003; Du et al. 2018).

A primary use of rest-UV spectroscopy is the study of the Lyα emission line. Because Lyα is a resonant line transition in neutral hydrogen its profile is complicated by the existence of even small amounts of neutral hydrogen within a galaxy. However, this also makes Lyα a good tracer of the covering fraction of neutral hydrogen (e.g. Matthee et al. 2021b). The escape of Lyα photons is also used as a proxy of the Lyman continuum escape fraction which is relevant for the ionizing background radiation of the intergalactic medium (e.g. Matthee et al. 2021a). Saldana-Lopez et al. (2022) have suggested a correlation between the Lyman continuum escape fraction and the EW of the low-ionization interstellar (LIS) absorption lines. moreover several studies (Jones et al. 2012; Berry et al. 2012; Shibuya et al. 2014; Oyarzún et al. 2017, etc.) have shown an anti-correlation between Lyα EW and LIS EW. Together this suggests greater amounts of Lyman continuum photons escaping from galaxies with higher Lyα EW and lower LIS absorption EW. Because Lyα emitters (LAEs) are typically less massive (e.g. Cullen et al. 2020; Pucha et al. 2022) this may imply greater Lyman continuum escape fractions for low mass galaxies. However, there remains to be a study of a complete sample of low-mass galaxies to confirm this trend.

Some ions in the ISM have ionization potentials lower than that of neutral hydrogen and therefore typically exist within regions of neutral hydrogen of sufficient column density to shield these ions from hard radiation. Because of this, these lines are often used to trace the outflows of neutral gas in the ISM (Shapley et al. 2003; Steidel et al. 2010; Jones et al. 2012; Hashimoto et al. 2013; Du et al. 2018; Sugahara et al. 2019). Generally speaking the typical velocity offset of LIS absorption lines remains the same across galaxy properties studied in the literature and is found to be ~ -180 km s^{-1} (Steidel et al. 2010; Hashimoto et al. 2013; Shibuya et al. 2014). LIS absorption equivalent width (EW) is also often correlated with Lyα EW (Jones et al. 2012; Du et al. 2018) such that weaker absorption is associated with stronger Lyα emission. This likely implies greater avenues of escape for Lyman continuum radiation. In fact, Saldana-Lopez et al. (2022) show an anti-correlation between LIS absorption EW and the escape fraction of Lyman continuum radiation. All of these properties are well studied at higher masses ($> 10^9$ M$_\odot$, Shapley et al. 2003; Berry et al. 2012; Jones et al. 2012; Du et al. 2018) or for samples chosen to have large Lyα EWs (e.g. Hashimoto et al. 2013; Shibuya et al. 2014), but little work has been done on a complete sample (in terms of star-formation rate) at low-masses to see if these trends hold for dwarf galaxies.

Outside regions of dense neutral hydrogen the elements can be subject to harder radiation and more highly ionized ions can be produced. These ions have ionization potentials well above that of neutral hydrogen and therefore will trace ionized regions of the ISM. Shapley et al. (2003) show that the HIS absorption line EW is constant in all there non-LAE bins, but in their LAE bin the HIS EW decreases in absolute value. Du et al. (2018) show

similar behavior for their $z \sim 2$ sample with the highest Lyα EW bin having weaker HIS absorption, arguably due to greater numbers of Lyα emitters contributing to the stack in that bin. Both argue that there is an insignificant change in the HIS EW strength with Lyα EW, but each display a sudden change in the strength of the HIS EW for LAEs. Since LAEs are less massive than Lyman break galaxies (LBGs) generally (e.g. Cullen et al. 2020; Pucha et al. 2022) it may be the case that lower mass galaxies have lower HIS EWs.

In this work we utilize photometric and spectroscopic data to study the UV spectral properties of dwarf galaxies and compare with the better-studied more massive galaxies. The remainder of the paper is organized as follows. In §3.2, we briefly review the observations and describe additional spectral energy distribution (SED) fitting, sub-sample selection, and describe the spectral stacking methodology. In §3.3, we present measurements of the Lyα, LIS, and HIS EWs and velocity offsets. In §3.4, we compare with measurements found in the literature and discuss the implications of these comparisons. In §3.5, we summarize our findings. We adopt a ΛCDM cosmology with $\Omega_m = 0.3$, $\Omega_\Lambda = 0.7$, and $h = 0.7$ throughout the paper and all magnitudes are in the AB system (Oke & Gunn 1983). In this work all EWs are given in the rest frame. emission lines are taken to have positive EWs and absorption lines are taken to have negative EWs. We use the convention of positive velocities indicating a redshift and negative velocities indicating a blueshift.

3.2 Observations, Data Reduction, and Sample Selection

3.2.1 Observations & Data Reduction

This work is based on data discussed in Snapp-Kolas et al. (2022) and the details of the observations and reduction can be found therein. We briefly review the basics of the sample here. Our sample consists of a subset of dwarf galaxies observed with deep HST photometry and low resolution rest-UV spectroscopy with Keck/LRIS (Oke et al. 1995). All of our galaxies are behind three lensing clusters (Abell 1689, MACS J1149, and MACS J0717) in order to observe the faintest UV continua possible with LRIS. Exposure times varied from 4500s-13000s in our 11 masks according to the conditions during observations. The typical seeing of our data is $\sim 1''$. Objects were selected to have visual magnitudes brighter than $m_{F625W} < 26.3$ and photometric redshifts in the range $1.5 < z < 3.5$. Photometric redshifts are determined from our HST photometry (see Alavi et al. 2014, 2016, for details). Galaxies with high magnification were given priority when creating slit masks. The LRIS data were reduced and extracted using a modified version of the PypeIt v1.x reduction pipeline (Prochaska et al. 2020), which performs flat-fielding, wavelength calibration, cosmic ray rejection, sky subtraction, and optimal extraction of 1D spectra. We correct these extracted spectra for slit-losses using Hubble photometry. The spectral coverage is 3100 Å-5600 Å and the spectral resolution is R $\sim$ 500. After removing spectra with contamination from internal reflections we have a parent sample of 127 spectra. After combining multiple images we have a parent galaxy sample of 89 galaxies. Keck/MOSFIRE (McLean et al. 2010, 2012) rest-optical spectra were also obtained for a portion of these galaxies, which we use to confirm the redshifts and measure the Hα emission line of the galaxies used

in this work. The details regarding the MOSFIRE spectra can be found in Gburek et al. (2022), but we shall summarize the spectroscopy here as well. The spectra were observed using a 2.5″ ABBA dithering pattern in the Y-,J-,H-, and K-bands with targets selected to have typical strong nebular emission lines (i.e. [OII] $\lambda\lambda$3726, 3729, Hβ, [OIII] $\lambda\lambda$4959, 5007, Hα, and [NII] $\lambda\lambda$6548, 6583) in 9 masks. The average exposure times for the Y-, J-, H-, and K-bands were 96 min., 81 min., 85 min., and 82 min. with resolutions of R = 3388, 3318, 3660, and 3610 respectively[2]. The spectra were reduced using the MOSFIRE Data Reduction Pipeline[3] (DRP). 1D spectra were then extracted from the reduced 2D spectra using `BMEP`[4] from Freeman et al. (2019).

3.2.2 SED fit

We fit SEDs to our galaxies within the IR footprint of our Hubble photometry in Alavi et al. (2014, 2016). In that work we make use of the code `FAST`[5] (Kriek et al. 2009) and we fit Bruzual & Charlot (2003) stellar population synthesis (SPS) models assuming constant star formation histories (SFHs), a Chabrier (2003) initial mass function (IMF), stellar metallicities of either $0.2Z_{\odot}$ or $0.4Z_{\odot}$, and an SMC dust attentuation curve. Three galaxies in this sample for this work did not have SED fits, as they were not observed in all of the filters of the Alavi et al. (2014, 2016) sample. Nevertheless, the photometry was sufficient for performing SED fits. For these galaxies we made use of `BAGPIPES`[6] (Carnall

[2] https://www2.keck.hawaii.edu/inst/mosre/grating.html

[3] https://keck-datareductionpipelines.github.io/MosreDRP/

[4] https://github.com/billfreeman44/bmep

[5] https://w.astro.berkeley.edu/~mariska/FAST.html

[6] https://bagpipes.readthedocs.io/en/latest/index.html

et al. 2018) to perform SED fitting on these galaxies. The same assumptions were used as in `FAST`, but a Kroupa (2004) IMF is used instead as this is fixed in the `BAGPIPES` code. We note that the Chabrier (2003) and Kroupa (2004) IMF's differ primarily at the low mass end ($\log(M^*/M_\odot) < 1$), and differences in the two are small in terms of the number of stars of a given mass. Therefore, we argue that the two assumptions will have little difference in the estimated mass which is the primary use of the SED fits in this work.

3.2.3 Sub-sample Selection

For the purposes of this study we aim to choose a sample that is complete in terms of its star-forming properties. We place the following constraints on our sample to accomplish this goal (Snapp-Kolas et al. 2022):

- Only galaxies with confirmed redshift from our rest-optical spectra are kept. These redshifts are determined from Hα and [OIII]$\lambda\lambda$5007.
- We require that Hα be observable within the MOSFIRE H, J, or K bands. This limits our observations to galaxies with $z \lesssim 2.6$.
- We remove galaxies that show blending with other nearby galaxies in the HST photometry
- We remove galaxies with magnification $\mu > 30$ behind Abell 1689 and $\mu > 15$ for MACS J0717 and MACS J1149. This is to ensure the galaxies in the sample are sufficiently far away from the critcal line, to avoid differential magnification across a galaxy.

- We remove galaxies with large slit losses (defined empirically to be a factor of greater than 2.2 in the LRIS and MOSFIRE spectra). Corrections larger than this may not be representative of the true spectrum of the galaxies, as a majority of the galaxy light lies outside of the slit.

- We additionally remove any galaxies that have an Hα/UV ratio at the low end of the observed range in our higher mass galaxies (see Snapp-Kolas et al. 2022, for the high-mass galaxies) and could not have been detected in Hα below the extrapolated star-forming main sequence of Sanders et al. (2021) given the sensitivity of our keck/MOSFIRE spectra. This is done to remove a bias towards galaxies that have large Hα luminosities.

Figure 3.1 shows the star-formation rate (SFR) vs. stellar mass of the remaining sample after the above considerations. The galaxies that have red x's could NOT have been detected in Hα below the main sequence and are therefore removed from the sample. Points are color-coded according to their magnification and the gold star represents the median SFR and Mass of the sample. The error bars on the star represent the 25th and 75th quintiles of the sample for each variable. Error bars on the individual galaxies are derived from the SED fits. These considerations leave us with a final complete sample of 16 dwarf galaxies. The sample is consistent with lying on the main sequence within 1σ of the Sanders et al. (2021) relation.

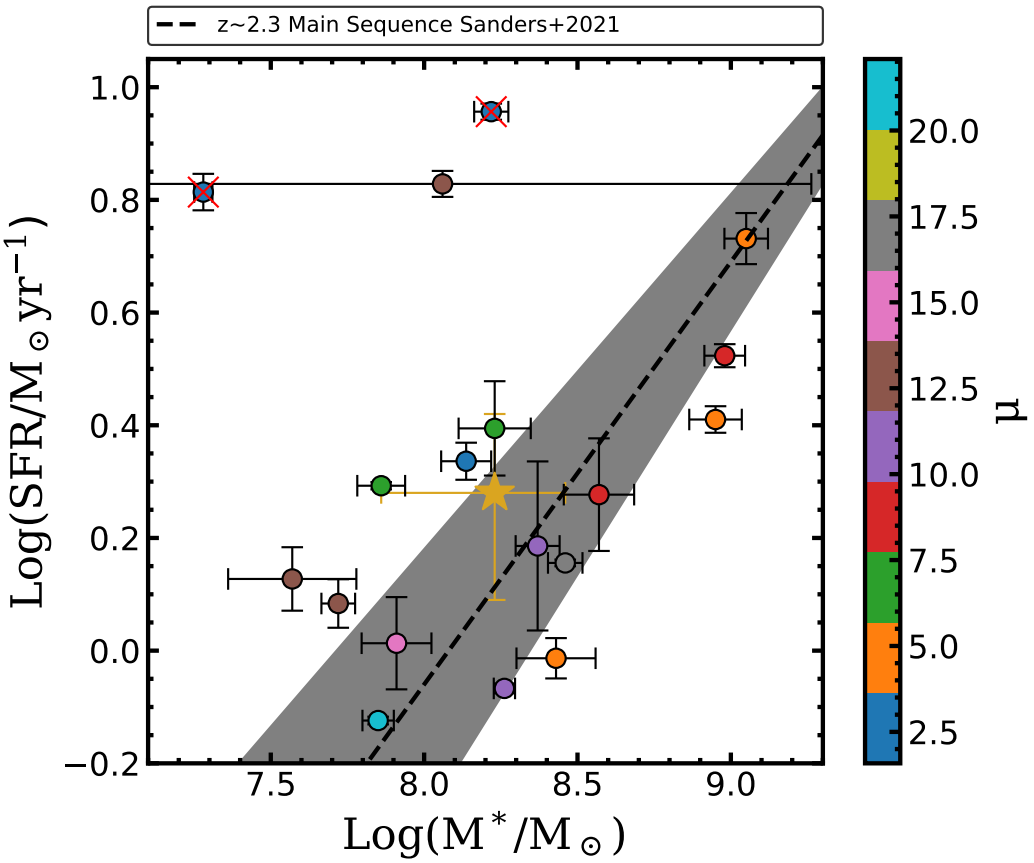

Figure 3.1: Galaxy main sequence for our dwarf galaxy sample. Points are color coded according to the magnification of each galaxy (see color bar). The main sequence extrapolated from the empirical Sanders et al. (2021) relation (eq. (3) in their paper) is plotted for reference along with the 1σ errors shaded in grey. The errors on the individual measurements are derived from the SED fitting codes. The median SFR and mass are plotted together with a golden star. The error bars on the star represent the 25th and 75th percentiles of the sample. Galaxies excluded because they would have Hα luminosites below our Hα sensitivity limit (adjusted by redshift and magnification) are marked with red x's.

3.3 Results

Thanks to lensing we are able to probe down to $M_{UV} \lesssim -17$ at $z \sim 2$, which is two orders of magnitude fainter than the KBSS sample ($M_{UV} \lesssim -19$) of Du et al. (2018). However, given the low luminosities of our sample, the S/N in the continuum is still too low to detect the LIS and HIS absorption features in individual spectra. Therefore, with the above sample we perform a median stack of all the galaxies to produce a typical dwarf galaxy spectrum to compare with larger mass galaxies. We normalize the individual spectra according to a power law of the form $f_\lambda \sim \lambda^\beta$ before stacking. Because the sample consists of galaxies at various redshifts between 1.6 and 2.6 the spectral coverage of the stack is limited to 1200 Å to 1560 Å.

Each spectrum in the stack contains statistical uncertainty given by the error spectrum. However, galaxies have a wide range of properties and given the size of our sample there is likely inherent variance in the stack do to this variance in galaxy properties. To account for both the statistical uncertainty and the variance in galaxy properties we perturb each spectrum according to its error spectrum and randomly select with replacement from our sample. We then median stack these mock spectra. We repeat this process 100 times and then take the standard deviation of the flux at each wavelength to be the error spectrum of our median stack. We use this error spectrum to produce the errors on our measurements of the absorption lines and the Lyα emission line. The normalized stack is shown in figure 3.2 along with the normalized z $\sim$ 2 stack of Du et al. (2018).

Our stacked spectrum spans the rest-frame wavelength range of 1200 Å-1560 Å and therefore probes the absorption lines of low and high ions and common emission lines

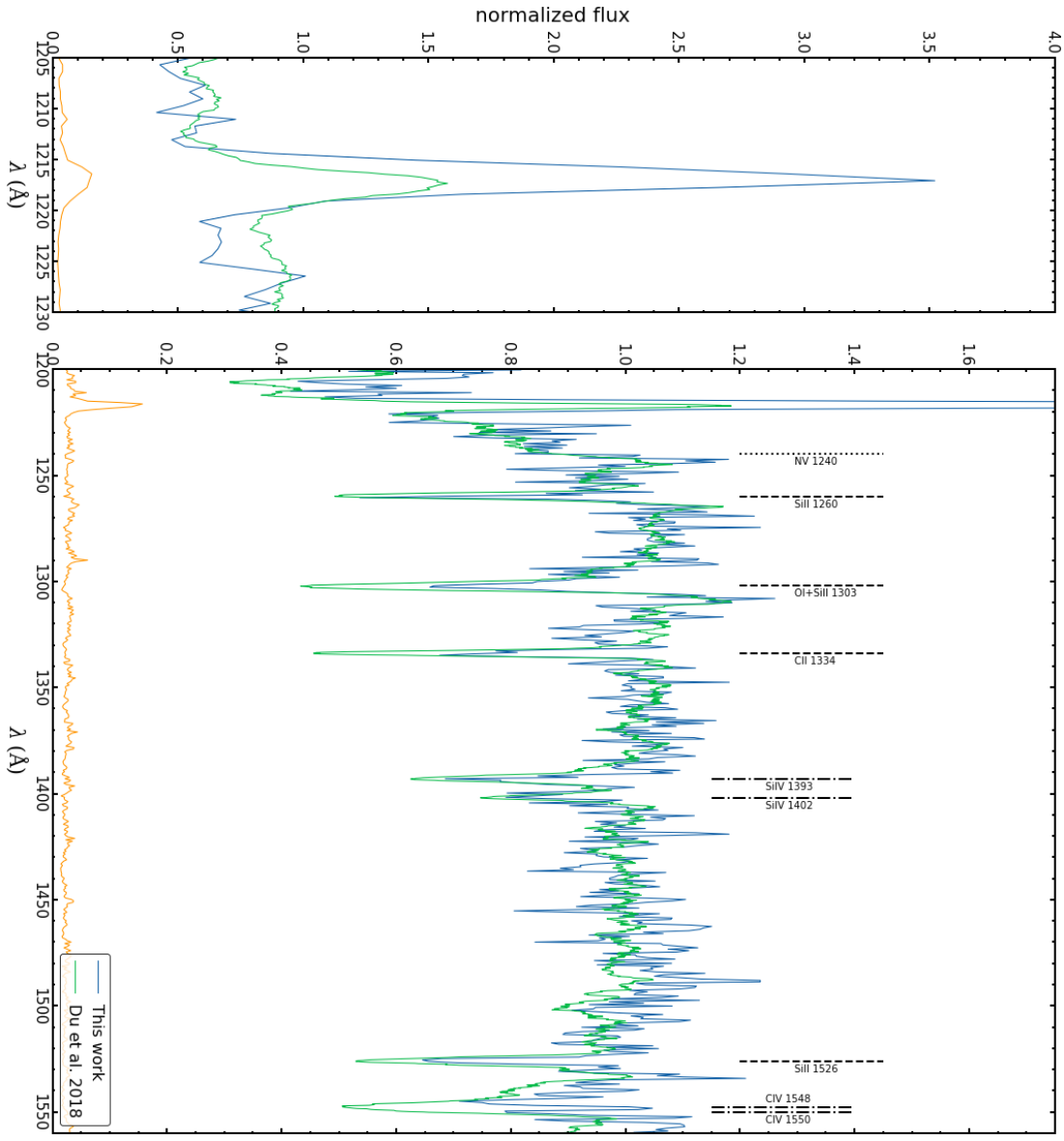

Figure 3.2: The stacked spectrum of the 16 dwarf galaxies in our sample is plotted in blue. The $z \sim 2$ stack of Du et al. (2018) is plotted in green. To compare the depths of the absorption lines we normalize the spectrum of Du et al. (2018) by the continuum, which we estimate using a running average with a width of 100 Å. The error spectrum is plotted in orange and relevant lines are labeled in the figure. Low-ionization absorption lines are labeled with dashes, high ionization lines are labeled with dot-dashes, and the NV line is labeled with a dotted line. Left: A comparison of the Lyα emission line. Right: the rest-UV continuum and absorption lines of the same stacks. Generally, the Lyα emission line is stronger, the LIS absorption lines are weaker, and the HIS absorption lines are weaker than the Du et al. (2018) stack.

such as the Si II fine structure emission lines, CIV emission, and N V λ1240. We also are able to measure the Lyα emission line EW and velocity offset relative to systemic to compare with Du et al. (2018).

We measure the LIS absorption lines by performing a parametric fit of the Si II λ1260, O I λ1302+Si II λ1304, C II λ1334, and Si II λ1527 lines. We assume Gaussian profiles and require the offset from systemic and the width of the lines to be the same for each LIS absorption line. This naturally presumes that all of the low ions occupy the same region of the galaxy. We use this model in a Markov Chain Monte Carlo procedure with PyMC3 to fit the lines to the data. This method takes into account the error spectrum on the medium stack described in section 3.2 and our measurement errors are taken from this fitting procedure. The HIS absorption lines are fit using a similar method but centering the Gaussian profiles on Si IV $\lambda\lambda$1393, 1402 and C IV $\lambda\lambda$1548, 1550 and not requiring the two to be at the same velocity shift or have the same width as in Shapley et al. (2003) and Du et al. (2018). The SiIV doublet is spectrally resolved, but the CIV doublet includes a P-Cygni profile that originates from stellar winds in massive stars. This makes it difficult to disentangle the stellar and interstellar components of the CIV profile (Du et al. 2018). Additionally, Rudie et al. (2019) observe a different profile for CIV in their L* galaxies, suggesting it traces an additional phase of the gas. Because of this, the CIV doublet may not be probing the same region of the galaxy as the SiIV doubet.

We fit the Lyα EW according to the methods of Du et al. (2018), which we briefly review here. We take the continuum to be the midpoint flux of a line passing through the flux at 1208 Å and 1240 Å. We then integrate from 1208 Å to 1240 Å to calculate the

EW (see Snapp-Kolas et al. 2022, for more details). To get the velocity offset of the Lyα profile we parameterize according to a Gaussian on top of a linear continuum. The same MCMC method used for the LIS absorption lines is used for this fit. Our measured EWs and velocity offsets from systemic are listed in table 3.1. Given our limited resolution in our composite spectrum we are unable to properly characterize the maximum velocity of our galaxies (Keerthi Vasan G. et al. 2022). We choose instead to fit a single Gaussian profile to each of our lines and use the line center of the fit to represent the outflow velocities of our galaxies do to our low-resolution spectroscopy ($R \sim 500$). We also measure $\mathrm{EW_{LIS}}$ which we define as the mean EW of the Si II λ1260, O I λ1302+Si II λ1304, C II λ1334, and Si II λ1527 absorption lines. We define it this way in order to compare with the literature which typically defines $\mathrm{EW_{LIS}}$ as such (e.g. Berry et al. 2012; Jones et al. 2012; Du et al. 2018; Saldana-Lopez et al. 2022). We measure $\mathrm{EW_{LIS}}$ to be -0.95 $\pm$0.03 Å for the total stack. We also find that the Lyα EW is 10.3 $\pm$0.2Å and the Lyα velocity offset from systemic is 319 $\pm$22 km $\mathrm{s^{-1}}$. The HIS absorption line EW is measured from the average of the SiIV doublet and is found to be -0.66 $\pm$0.04 Å.

3.4 Discussion

To study the mass dependence of properties of dwarf galaxies at a given redshift we compare primarily with the KBSS sample of Du et al. (2018).

Table 3.1: The emission and absorption line EWs and velocity offsets from systemic measured from the total median stack of 16 dwarf galaxies. We take the convention of positive velocity indicating a redshift and negative velocities indicating a blueshift.

line (Name)	EW (Å)	EW_{err} (Å)	v (km s^{-1})	v_{err} (km s^{-1})
Lyα	10.3	0.2	319	22
SiII 1260	-0.81	0.05	-121	10
OI 1302 + SiII 1304	-1.20	0.06	-117	9
CII 1334	-0.83	0.05	-114	9
SiII 1526	-0.99	0.04	-100	8
SiIV 1393	-0.89	0.07	-73	20
SiIV 1402	-0.43	0.05	-72	20
CIV 1548[1]	-0.76	0.07	-573	18
CIV 1550[1]	-0.01	0.01	-572	18

[1] It is unclear whether the absorption features in the stack are in fact CIV. It is possible that there are large amounts of "filling in" at low velocities from emission from the P-Cygni stellar wind profiles.

3.4.1 Lyα

Figure 3.3 shows the Lyα EW as a function of stellar mass. Du et al. (2018) demonstrate a relatively flat trend in $EW_{Ly\alpha}$ with mass down to $\log(M^*/M_\odot) \approx 10$. Below this mass they show an increase to $EW_{Ly\alpha} \approx 0$Å at $\log(M^*/M_\odot) \approx 9.5$. Our stack continues this trend demonstrating that Lyα will be seen in emission on average below $\log(M^*/M_\odot) \approx 9$. We see a clear increase in the Lyα EW with decreasing mass. Du et al. (2018) show that for a given stellar mass $EW_{Ly\alpha}$ will increase with redshift. This is particularly stark at the lowest masses and may suggest that galaxies at the masses of our sample are Lyα emitters (LAEs, $EW_{Ly\alpha} > 20$Å) on average at $z \geq 4$. This suggests that lower mass galaxies

allow greater amounts of Lyα photons to escape, and therefore suggests greater amounts of ionizing radiation escape. This trend towards higher Lyα EWs at lower mass is also observed in other high-redshift samples in the literature (see for e.g. Oyarzún et al. 2017, $3 < z < 4.6$).

We also compare samples to determine trends in Lyα EW with absolute UV magnitude. Figure 3.4 is color coded in the same manner as figure 3.3. According to Du et al. (2018) there is a flat trend for $z \sim 2$ galaxies in $EW_{Ly\alpha}$ with M_{UV} and each bin shows that Lyα is observed with net absorption. In our dwarf galaxy sample we find a positive Lyα EW, showing that the typical dwarf galaxy will have net Lyα emission. This is consistent with our earlier work as well (Snapp-Kolas et al. 2022). However, at higher redshift in the Du et al. (2018) sample there is a noted increase in Lyα EW towards fainter absolute UV magnitudes. With our sample added to the analysis of Du et al. (2018) we can conclude that at redshifts $z \sim 2 - 4$ fainter galaxies produce higher Lyα EWs, and generally there exists an absolute UV magnitude at which the typical galaxy shifts from being a net absorber of Lyα photons, to being a net emitter of Lyα photons.

Patches of neutral hydrogen will greatly attenuate the Lyα line strength. Given low-ionization ions exist within regions of neutral hydrogen we expect the strength of Lyα to be tightly correlated with the strength of the LIS absorption lines. Figure 3.5 shows the LIS EW as a function of the Lyα EW. At the redshift of our sample, Du et al. (2018, blue) show a clear correlation between the LIS absorption line EW and the Lyα EW. They offer that this supports a physical model of patchy optically thick clumps surrounding star-forming regions. In this scenario the trend between the LIS EW and the Lyα EW is an

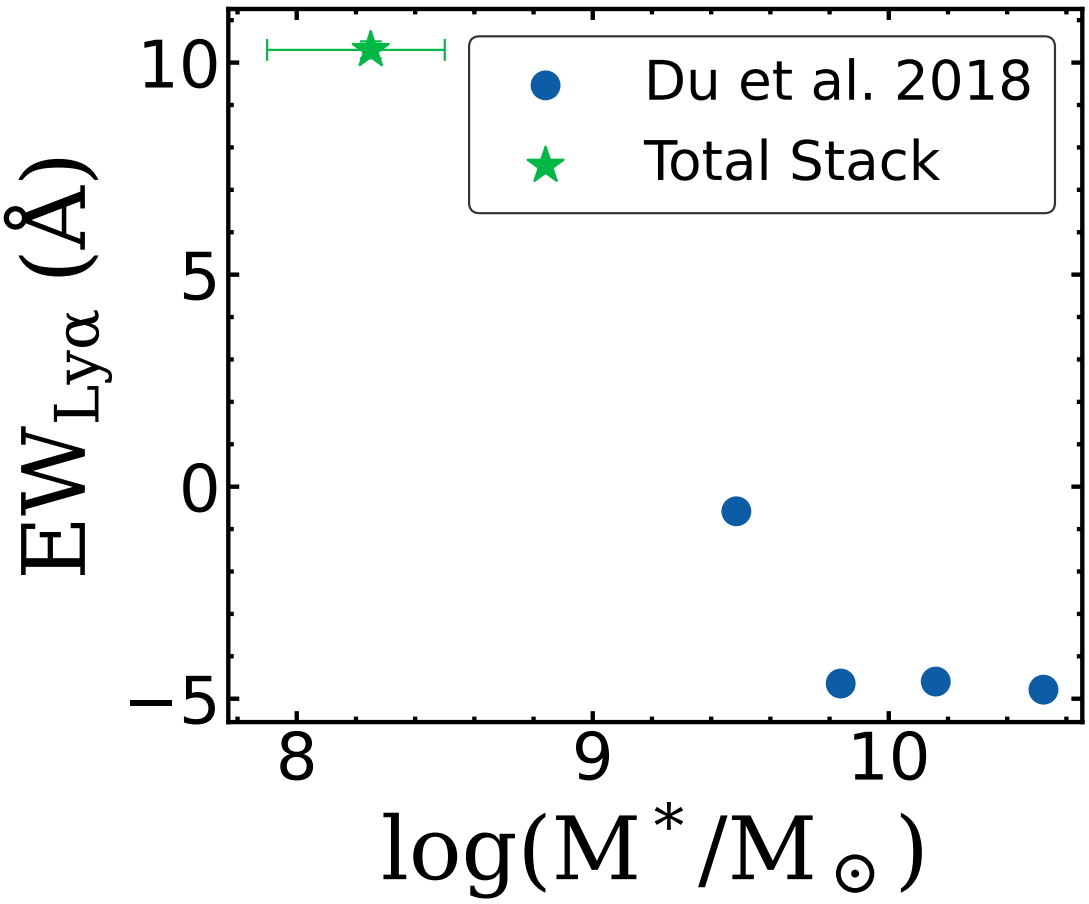

Figure 3.3: $EW_{Ly\alpha}$ vs. $\log(M^*/M_\odot)$ from stacked spectra at $z \sim 2$. Our datum is shown as a green star and the Du et al. (2018) data are shown in blue circles. The sample of Du et al. (2018) is binned according to mass and spectra are stacked in each mass bin. The errors on the KBSS sample are too small to be seen in the figure. For our dwarf galaxy sample the error bars on the Lyα EW are derived from the MCMC fit to the Lyα line as described in section 3.3. The error bars on the mass denote the 25th and 75th percentiles of the distribution respectively. The measured mass value is the median of the total sample. There is a clear increase in $EW_{Ly\alpha}$ with decreasing mass.

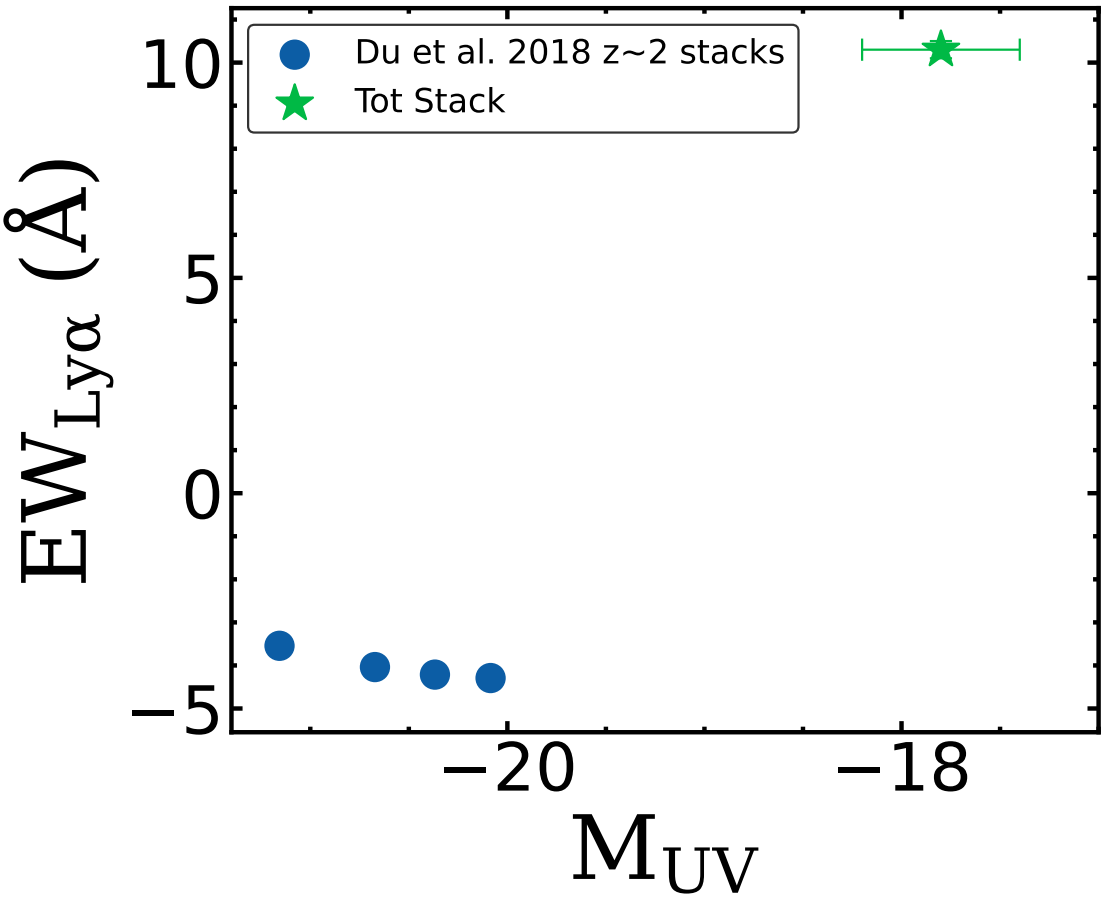

Figure 3.4: The $EW_{Ly\alpha}$ vs. M_{UV} from stacked spectra at $z \sim 2$. The green star is the measurement from our stack and the blue dots are from Du et al. (2018). Here the Du et al. (2018) sample is binned according to absolute UV magnitude. Again the error bars on the Du et al. (2018) sample are too small to be perceived in the figure and our error bars are calculated in the same manner as in figure 3.3. The error bars on the absolute UV magnitude are the 25th and 75th percentiles of the sample. There is a clear increase in the $EW_{Ly\alpha}$ at fainter UV luminosies

emergent property of the radiative transfer of Lyα photons. Du et al. (2018) demonstrate that this correlation is invariant up to $z \sim 4$. Pahl et al. (2020) extend the study of Du et al. (2018) out to $z \sim 5$ and find this correlation as well, though it may begin to flatten out at higher redshift. Shibuya et al. (2014, purple) continue the trend seen by Du et al. (2018) at higher Lyα EWs and also suggest that this correlation is indicative of a patchy distribution of neutral hydrogen. Berry et al. (2012, red) are also consistent with this trend. At higher redshifts, Jones et al. (2012, orange) show a clear trend of weaker LIS absorption with stronger Lyα emission. They suggest that this is consistent with a trend towards weaker LIS absorption and stronger Lyα emission in galaxies with fainter UV luminosities. They also find possible offsets in this trend based on the UV-spectral slope of the galaxies. redder galaxies have stronger LIS absorption at fixed Lyα EW. Saldana-Lopez et al. (2022, green) also observe this tight correlation between the LIS absorption EW and the Lyα EW and agree with the physical picture of a patchy distribution of neutral hydrogen traced by LIS absorption lines.

We find smaller absolute values of LIS EW at a given Lyα EW for our sample than those of Du et al. (2018), Berry et al. (2012), and Shibuya et al. (2014). This suggests that the trend between LIS EW and Lyα EW found in Du et al. (2018) is dependent on stellar mass or UV luminosity as argued by Jones et al. (2012).

However, we have stacked on the entire sample for this comparison. In order to more closely compare with the literature we stack two sub-samples chosen on Lyα rest-EW as is done in these other works. We split the sample by the median Lyα EW (6.2 Å). Each sample has 8 galaxies in the bin and they are stacked in the same manner as the full

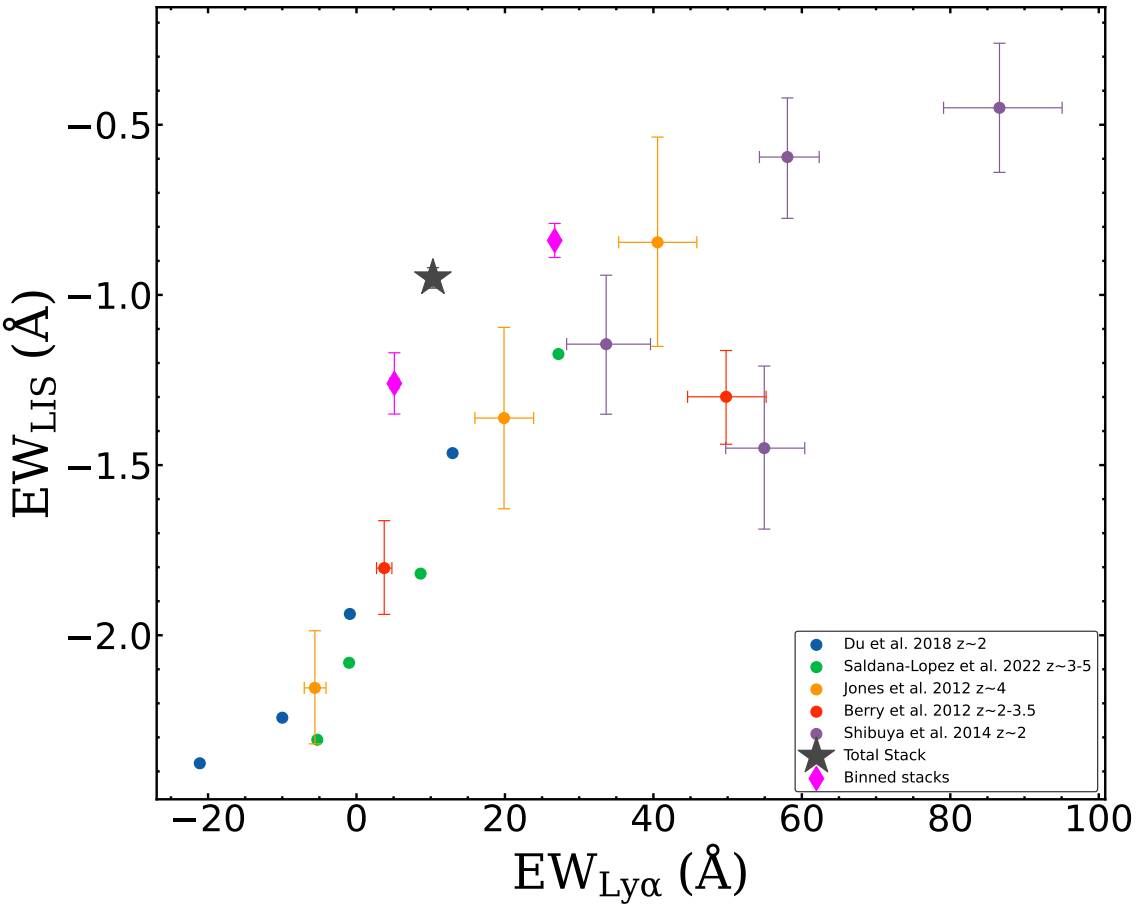

Figure 3.5: The $\mathrm{EW_{LIS}}$ vs. $\mathrm{EW_{Ly\alpha}}$ of high-redshift star-forming galaxies. The black star is measured from our total stack with the error on $\mathrm{EW_{LIS}}$ determined from the MCMC fitting algorithm (with error spectrum taken into account) and the error on $\mathrm{EW_{Ly\alpha}}$ is determined by propagation of error from the error spectrum. The pink diamonds are stacks on 8 galaxies each from our sample of 16 galaxies in two bins of $\mathrm{EW_{Ly\alpha}}$ split at 6.2 Å. The errors are determined in the same manner as the total stack. We also plot values from Du et al. (2018), Jones et al. (2012), Berry et al. (2012), Shibuya et al. (2014), and Saldana-Lopez et al. (2022) in blue, orange, red, purple, and green respectively for comparison with our sample. Each sample bins on $\mathrm{EW_{Ly\alpha}}$, and measures values from stacks within the bin, except for Saldana-Lopez et al. (2022) whose values come from individual LAEs. All of the literature values show a correlation between $\mathrm{EW_{LIS}}$ and $\mathrm{EW_{Ly\alpha}}$ for $\mathrm{EW_{Ly\alpha}} < 45$ Å. The measurements from our stacks lie marginally above the trends from the literature.

sample and the error spectrum is found in the same manner as well. All measurements are performed the same as for the total stack. The results are plotted as pink diamonds in figure 3.5. Our data lie above the trend in the literature, suggesting the relationship between $EW_{Ly\alpha}$ and EW_{LIS} may be mass dependent. However, Du et al. (2021) investigate this trend using individual galaxy measurements in order to investigate possible drivers of the scatter in this and other correlations. They find that for a fixed Lyα EW the LIS EW will vary based on the metallicity of the galaxy, with weaker LIS absorption occuring in lower metallicity galaxies. As such, the offset in our data may be indicative of our galaxies having lower metallicities.

3.4.2 LIS Absorption Lines and Kinematics

We wish to understand the distribution of neutral hydrogen to better constrain the escape of ionizing radiation. Here we compare our results with the KBSS sample of Du et al. (2018) to find any trends in the LIS absorption lines with mass. The kinematics of ions/gas are often characterized either by the centroid velocity of the absorption line or some choice of maximum velocity offset in the absorption line profile. The maximum velocity offset is often chosen to be at 90% flux relative to the continuum value (e.g Sugahara et al. 2017; Weldon et al. 2022). However, given the resolution of our spectra we choose to use the centroid as described in section 3.3. Figure 3.6 shows the LIS absorption velocity offset from systemic as a function of mass. To compare with the literature we take the CII 1334 velocity offset to be representative of the LIS absorption lines generally. There is a clear trend towards lower LIS absorption velocity offsets at lower masses relative to higher mass samples (Du et al. 2018; Sugahara et al. 2019). The models from the FIRE

simulations Muratov et al. (2015) predict that the outflow velocities will be lower in lower mass galaxies. Our results are qualitatively consistent with this model.

Figure 3.7 shows the LIS EW as a function of mass. Du et al. (2018) measure a single value of the LIS EW relative to mass ($EW_{LIS} \approx -2.0$Å). According to figure 3.5 (see also Du et al. 2018, figure 5) there is little to no dependence on the LIS absorption line EW with redshift. Therefore, there should be little variance in any relation with mass due to redshift. With this in mind we also compare with Jones et al. (2012) and Harikane et al. (2020) and observe an apparent anti-correlation. Our datum shows weaker LIS EW at lower mass and further indicates an anti-correlation between LIS EW and mass. Given this we fit an empirical relation between the LIS absorption EW and the log stellar mass of the form:

$$EW_{LIS} = a_1 \log(M^*/M_\odot) + a_2 \tag{3.1}$$

We make use of numpy's polyfit algorithm to perform a least squares fit of this relation to the observed data. We find $a_1 = -0.55 \pm 0.11$ and $a_2 = 3.7 \pm 1.1$. The best fit line is plotted in figure 3.7. Additionally, we observe the ratio of silicon lines to be $EW_{SiII1260}/EW_{SiII1526} = 0.8 \pm 0.1$, which is consistent with the LIS gas being optically thick and the absorption profiles being saturated. Since saturated LIS absorption lines trace neutral hydrogen covering fraction we conclude that lower mass galaxies have lower covering fractions.

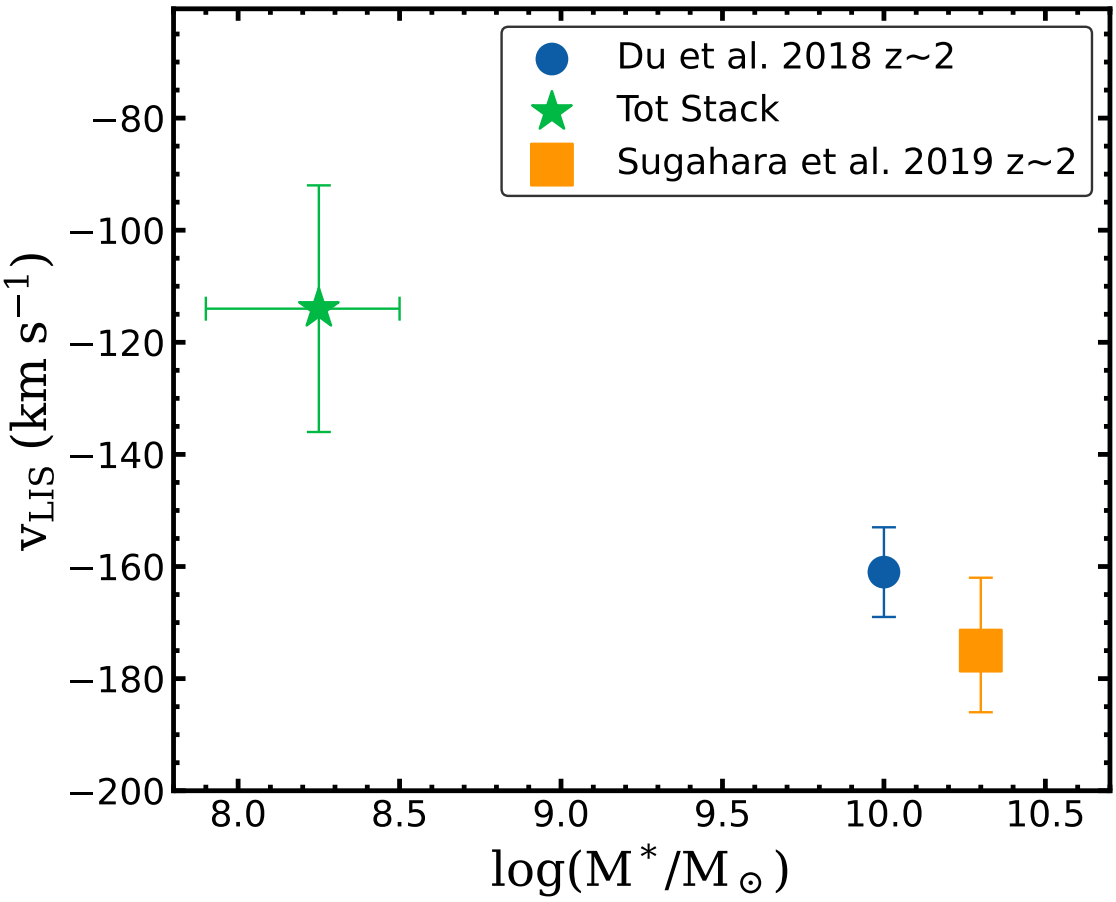

Figure 3.6: The LIS absorption velocity offset as a function of stellar mass. The green star is from our stack and the blue dot and orange square are from Du et al. (2018) and Sugahara et al. (2019) respectively. The errors on the mass for our stack are the same as in figure 3.3 and the errors on the velocity are derived from the MCMC algorithm that fit the lines to the spectrum. The measured LIS velocity is lower than Du et al. (2018) and Sugahara et al. (2019). The data point from Sugahara et al. (2019) is a correction of a measurement first made in Sugahara et al. (2017)

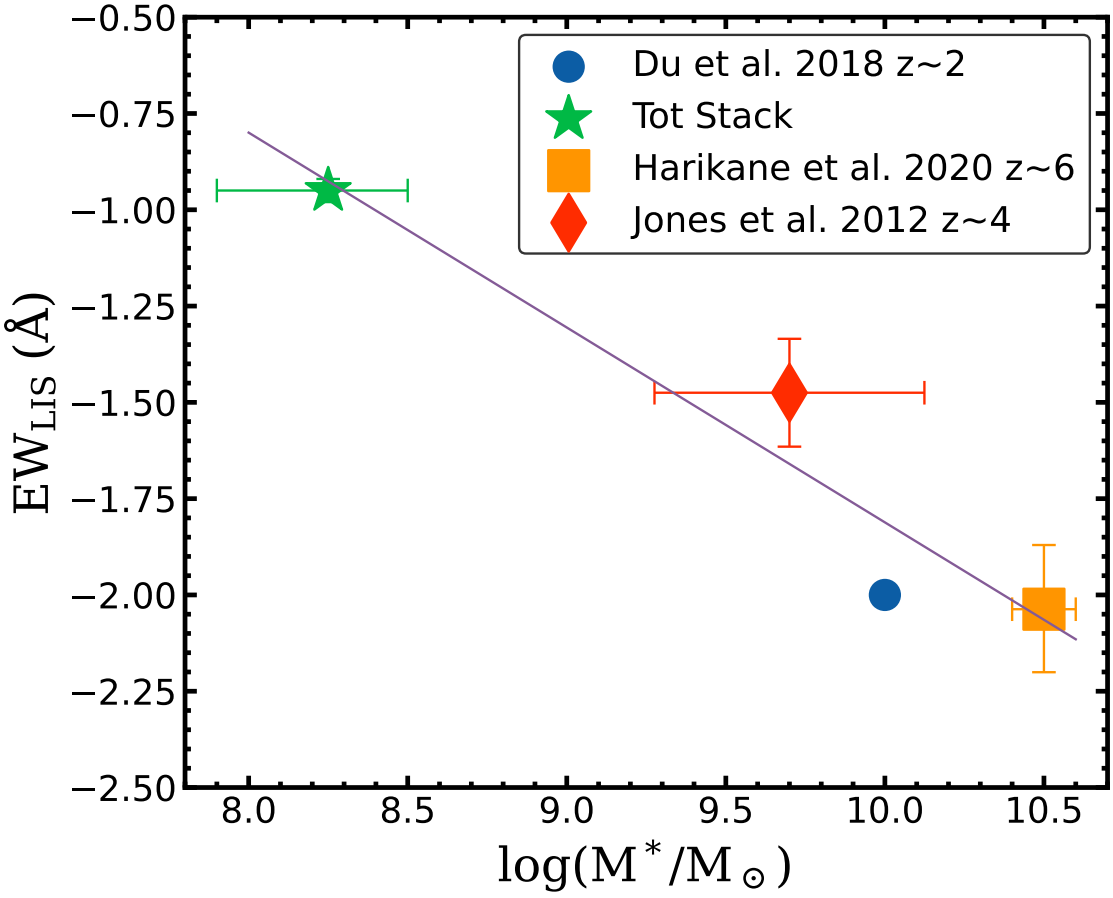

Figure 3.7: The EW_{LIS} as a function of stellar mass. The green star is our datum, the red diamond is from Jones et al. (2012), the blue dot is from Du et al. (2018), and the orange square is from Harikane et al. (2020). The errors on the mass are as in figure 3.3 and the errors on EW_{LIS} are derived from the MCMC fitting algorithm. We also plot a least-squares linear fit to the data points in purple showing that there exists an anti-correlation between EW_{LIS} and $\log(M^*/M_\odot)$.

3.4.3 HIS absorption lines

The relative abundance of high ions and low ions is indicative of the ionization state of the ISM. A more highly ionized ISM is likely to accommodate the escape of ionizing radiation. In figure 3.8 we plot the HIS absorption EW against mass. Du et al. (2018) measure the HIS EW to be ~ -1.4Å. We find the HIS EW of our dwarf galaxies to be about half as strong ($\mathrm{EW_{HIS}} = -0.66 \pm 0.04$Å). At higher redshift, Jones et al. (2012) measure a comparable value ($\mathrm{EW_{HIS}} \approx -1.5$) to Du et al. (2018) at similar mass. This is consistent with the higher redshift samples of Du et al. (2018), which suggest the HIS absorption strength doesn't change with redshift. Shapley et al. (2003) show that the LAEs of their sample have weaker HIS absorption than do the LBGs of their sample. It may be the case that this difference in their sample merely reflects a difference in the mass of LAEs and LBGs. We have shown that the Lyα EW increases with decreasing mass in agreement with other works in the literature. As such we may expect that a sample of LAEs will have lower masses than a higher mass LBG sample. However, we also make sub-stacks on Lyα EW and measure $\mathrm{EW_{HIS}} = -0.96 \pm 0.23$Å in our low Ly$\alpha$ EW stack and $\mathrm{EW_{HIS}} = -0.56 \pm 0.05$Å in our high Ly$\alpha$ EW stack. Therefore, we agree with Shapley et al. (2003) and Du et al. (2018) in that galaxies with high Lyα EW will have lower HIS EW. Given the uncertainty in our lower Lyα EW stack we can only state that the measurement is more consistent with our high Lyα stack than with the higher mass sample of Du et al. (2018). Together, this seems consistent with mass being the primary driver for lower HIS absorption EW. While the HIS EW appears to be anti-correlated with the mass of the galaxy the HIS velocity offset is less clear. We measure the velocity offset of our SiIV absorption lines to be -73 ± 20 km s^{-1}

and that of our CIV absorption lines to be -573 ± 18 km s^{-1}. The average of these two (-323 ± 13 km s^{-1}) is in good agreement with the offset measured in the literature (-220^{+150}_{-100}, Sugahara et al. 2019). This may suggest that the winds of the HIS absorption lines are primarily stellar in origin rather than nebular as they appear to not be effected by a change in mass. However, the profile of the CIV line in our stack is likely contaminated by the P-Cygni profile produced by stellar winds and may not be well fit by our model. Jones et al. (2012) suggest the use of the Si IV $\lambda\lambda$1393, 1402 doublet EWs as a means of tracing whether the HIS absorption is optically thick or not. If the ratio $W_{1393}/W_{1402} \sim 2$ then the gas is optically thin, but if $W_{1393}/W_{1402} \sim 1$ then the gas is optically thick. Jones et al. (2012) show a ratio of 1.4 ± 0.4 and argue that this means there is a significant amount of optically thick HIS gas present in their average galaxy. Additionally, Du et al. (2018) consistently measure ratios greater than 1 and suggest that this means the gas is at least partially optically thin. For our composite spectrum we measure $W_{1393}/W_{1402} = 2.07 \pm 0.28$ suggesting that the SiIV gas is optically thin in contrast with the higher mass samples of Jones et al. (2012) and Du et al. (2018).

3.5 Summary

In this paper we have studied the UV spectroscopic properties of the typical dwarf galaxy at $z \sim 2$ via stacking. The systemic redshift of the individual galaxies is constrained using our rest-optical MOSFIRE spectra. We fit the Lyα emission line and the LIS and HIS absorption lines using MCMC routines to measure the velocity offsets of these lines relative to the systematic redshift. We measure the EW of Lyα using the methods of Du

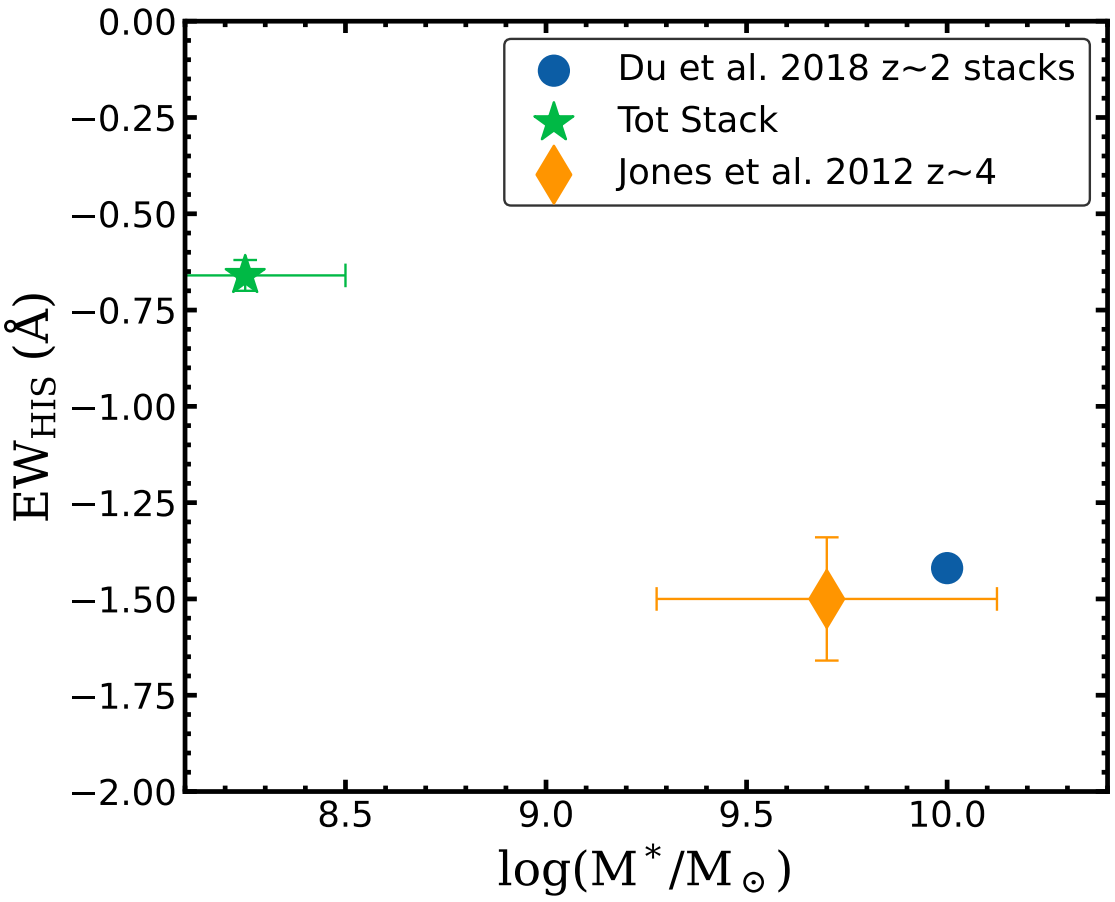

Figure 3.8: EW_{HIS} vs. stellar mass. The green star is our datum, the blue dot is from Du et al. (2018), and the orange diamond is from Jones et al. (2012). The errors on our datum are determined in the same manner as figure 3.7. At $z \sim 2$ there is less HIS absorption at lower mass. There is no indication of a change in the depth of the HIS absorption lines with redshift for high mass galaxies. Therefore, the depth of HIS absorption lines appear to depend primarily on mass and do not evolve with time.

et al. (2018), and we measure the EWs of the LIS and HIS absorption lines using the best fit model of the MCMC routines. We find the following primary results from these measurements:

- We find that the typical $EW_{Ly\alpha}$ is much larger for dwarf galaxies than for the higher mass galaxy sample of Du et al. (2018). This is in agreement with our earlier work (Snapp-Kolas et al. 2022).
- We find that the correlation in EW_{LIS} with $EW_{Ly\alpha}$ is offset towards lower absolute values of EW_{LIS} (i.e. less absorption) for dwarf galaxies. Possibly connected to dwarf galaxies having lower metallicities (Du et al. 2021).
- Lower mass galaxies have about half the EW_{LIS} of more massive galaxies. There is an anti-correlation between EW_{LIS} and mass. We find the following best fit values for the linear model: $EW_{LIS} = (-0.55 \pm 0.11)\log(M^*/M_\odot) + (3.7 \pm 1.1)$.
- We find velocity offsets in the LIS absorption lines for lower mass galaxies to be lower than in high mass galaxies in agreement with the FIRE simulations (Muratov et al. 2015).
- EW_{HIS} is smaller in absolute value than for higher mass galaxies.
- We find that the SiIV doublet is consistent with the gas being optically thin.

It is clear that dwarf galaxies have higher Lyα EWs, weaker LIS and HIS absorption EWs, and lower LIS velocity offsets relative to more massive galaxies. Larger Lyα EW's imply higher Lyα escape fractions (e.g. Yang et al. 2017) which may imply larger Lyman continuum escape fractions (Dijkstra et al. 2016; Verhamme et al. 2017; Izotov et al. 2020;

Flury et al. 2022). Similarly, Trainor et al. (2019) show that the Lyα escape fraction is anti-correlated with EW_{LIS} suggesting higher Lyman continuum escape for weaker EW_{LIS}. More directly, Saldana-Lopez et al. (2022) show that the Lyman continuum escape fraction is anti-correlated with $|EW_{LIS}|$. Our dwarf galaxies exhibit stronger Lyα and weaker LIS EWs relative to more massive samples. Therefore, dwarf galaxies likely have greater Lyman continuum escape fractions. More data at intermediate masses at $z \sim 2$ would help to clarify the relationship between EW_{HIS} and mass. These data could also be used to further solidify our results on the LIS absorption lines and Lyα.

Acknowledgments

This research made use of `PypeIt`[7], a Python package for semi-automated reduction of astronomical slit-based spectroscopy (Prochaska et al. 2020; Prochaska et al. 2020). Some of the data presented herein were obtained at the W. M. Keck Observatory, which is operated as a scientific partnership among the California Institute of Technology, the University of California and the National Aeronautics and Space Administration. The Observatory was made possible by the generous financial support of the W. M. Keck Foundation.

The authors wish to recognize and acknowledge the very significant cultural role and reverence that the summit of Maunakea has always had within the indigenous Hawaiian community. We are most fortunate to have the opportunity to conduct observations from this mountain Based on observations made with the NASA/ESA *Hubble Space Telescope*, ob-

[7] https://pypeit.readthedocs.io/en/latest/

tained from the Data Archive at the Space Telescope Science Institute, which is operated by the Association of Universities for Research in Astronomy, Inc., under NASA contract NAS5-26555. These observations are associated with programs #9289, #11710, #11802, #12201, #12931, #13389, #14209.

Data Availability

This paper is based on public data from the Hubble Space Telescope as well as from programs 12201, 12931, 13389, 14209. Spectroscopic data from our survey with the Keck Observatory. These data are available upon request from Christopher Snapp-Kolas or Dr. Brian Siana.

Chapter 4

Conclusions

We seek to better understand the mechanisms which dictate the formation and evolution of galaxies throughout cosmic time. In this work we narrow our focus to the escape of ionizing radiation and the mechanisms dictating the outflows of material from dwarf galaxies. These determine the ionizing background radiation and the star formation efficiency of dwarf galaxies. These phenomena have been well studied for high mass galaxies ($\log(M^*/M_\odot) > 9$) (e.g. Du et al. 2018, 2021) and for samples biased towards strong emission lines (e.g. Hayes et al. 2010; Weiss et al. 2021), but little work has been done for low-mass galaxies. We present a first look at a complete and representative sample of rest-UV spectra of lensed dwarf galaxies at $z \sim 2$. With this sample we constrain the escape of ionizing photons indirectly through an analysis of the Lyα EW distribution. Additionally, we constrain the outflows of dwarf galaxies via the absorption lines of low- and high-ionizing ions present in the ISM of the dwarf galaxies. A summary of our results from our study of 32 individual dwarf galaxies and the stack of 16 dwarf galaxies is presented here. We

contextualize our findings by comparing with higher mass and emission line based studies of star-forming galaxies at similar and higher redshifts.

The escape fraction of ionizing radiation is notoriously difficult to measure directly from spectroscopy (e.g. Siana et al. 2010; Grazian et al. 2016; Rutkowski et al. 2017). As such, indirect methods are employed to constrain the escape of ionizing radiation. One such method is to use the escape fraction of Lyα photons. Because Lyα is a resonant line it is argued that any avenue of escape for Lyα radiation will also be an avenue of escape for Lyman continuum radiation (e.g. Matthee et al. 2021b). In general, we are interested in the net escape of radiation in a population of galaxies. It is often the practice in the literature to look at the population of galaxies and determine the typical strength of the observed Lyα emission line. This is frequently characterized using the Lyα EW distribution. This distribution is well studied for high mass galaxy samples (e.g. Du et al. 2018) and shown to have net absorption in the Lyα line. However, the net escape of Lyα photons from all galaxies necessarily includes lower mass galaxies. In fact, according to the luminosity functions of Alavi et al. (2016), Konno et al. (2016), and Bouwens et al. (2022) the number of dwarf galaxies accounts for more than 50% of the UV luminosity density at $z \sim 2$. Therefore, dwarf galaxies likely contribute a large fraction of the ionizing radiation. Indeed, we find that the typical dwarf galaxy at $z \sim 2$ has Lyα in net emission. The median EW of the more massive galaxies is $\langle \mathrm{EW_{Ly\alpha}} \rangle = -6^{+1.9}_{-1.1}$ and that of dwarf galaxies is $\langle \mathrm{EW_{Ly\alpha}} \rangle = 9.6^{+3.0}_{-2.9}$ which differ by about 4σ. We also find that about 60% of the integrated Lyα luminsoity density comes from galaxies with Lyα EWs greater than 20 Å in dwarf galaxies. This means that, under the classical definition of Lyα emitters (LAEs,

$EW_{Ly\alpha} > 20$Å), the majority of Lyα photons are coming from LAEs. We would like to understand the underlying phenomena driving this distribution. To better understand this we measure the intrinsic Lyα EW.

To better understand the mechanisms by which we observe this increase in the typical observed Lyα EW we measure the intrinsic Lyα EW as a metric of the strength of the stellar populations. In the literature, the typical method of measuring the strength of the ionizing sources is through the ionizing photon production efficiency (ξ_{ion}) which measures the ability of the stellar populations to produce ionizing radiation irrespective of the escape of that radiation into the IGM (see Emami et al. 2020; Shivaei et al. 2018). Both ξ_{ion} and the intrinsic EW depend on the same observables and differ by multiplicative factors. The observables necessary for this measurement are the Hα emission line, which under case-B recombination has a roughly constant ratio with the Lyα emission line of 8.7, and the UV luminosity extrapolated to $\sim$ 1216Å (the wavelength of Lyα). Because we are looking for the intrinsic EW we must ensure that we are measuring the intrinsic Hα and UV luminosities. Each of these is attenuated by dust and so we correct each according to our dust measurements. For the Hα dust correction we make use of a typical dust correction based on the work of Gburek et al. (2022) which median stacked on a similar sample of dwarf galaxies to measure the metallicity of dwarf galaxies. From the median stack we find a value of $A_V = 0.54$ by use of the Balmer decrement. We then use a Cardelli et al. (1989) attenuation curve to correct the Hα emission line. We similarly correct the UV luminosity, but instead use A_V values derived from SED fitting and an SMC attenuation curve (Gordon et al. 2003) as this has been shown to be more accurate for bluer wavelengths

in high-redshift low-metallicity galaxies (Reddy et al. 2022). When we convert the average ξ_{ion} measurements in Shivaei et al. (2018) and Emami et al. (2020) to intrinsic Lyα EWs we find that our average intrinsic EW measurement for dwarf galaxies ($M_{UV} > -19$) is elevated (67 Å vs. 23 Å). However, this does not seem to be sufficient for producing high observed EW's in our sample. We find that even high intrinsic EW galaxies display low observed EW's. It is likely the case that significant amounts of the intrinsic output of these galaxies is being obscured either by dust or neutral hydrogen in the ISM. We investigate the attenuation of Lyα photons, and how this effects the EW distribution, via the Lyα escape fraction.

In order to have a positive (under our convention) Lyα EW it is necessary that some excess number of Lyα photons above the continuum escape from the galaxy. Because Lyα is a resonant line transition in the hydrogen atom it has a large cross-section for interaction with any hydrogen atoms. This means that even low-column density regions of neutral hydrogen can obscure Lyα radiation. Lyα photons also have large interaction cross-sections with dust molecules. Because of this it is necessary that there be at least some low-column density regions of a galaxy for Lyα photons to escape through. In recent years the picket-fence concept of the distribution of gas in star-forming galaxies has gained popularity (e.g. Matthee et al. 2021b). This concept argues for a scenario in which all gas in the galaxy is optically thick to Lyα radiation and that only low-column density "holes" in the gas allow the escape of Lyα photons. Some studies support this scenario by showing the ratio between low-ionization absorption lines of the same ion is ~ 1 when the theoretical ratio between the ions should be otherwise (Quider et al. 2010; Jones et al. 2013;

Harikane et al. 2020; Saldana-Lopez et al. 2023). Under this physical picture we can use the escape fraction of Lyα photons as a tracer of the covering fraction of neutral hydrogen in dwarf galaxies. generally speaking we find that the Lyα escape fraction correlates with the observed Lyα EW, with classically defined LAEs requiring escape fractions larger than 5%. Because low neutral hydrogen column density regions are necessary for the escape of Lyα radiation and the interaction cross-section for Lyman continuum photons is much lower than that of Lyα it is reasonable to presume that the escape fraction of Lyα will at least serve as an upper limit on the Lyman continuum escape fraction and the two may be correlated (Dijkstra et al. 2016; Verhamme et al. 2017; Izotov et al. 2020). As such we measure the volumetric Lyα escape fraction as well and find it to be $4.6^{+2.0}_{-1.4}$%. This can be used to place constraints on contributions from dwarf galaxies on the ionizing background radiation. While this gives a general overview of the properties of the ISM gas the HIS and LIS absorption features give us a more complete picture of the gas properties.

The evolution of galaxies across cosmic time is heavily dependent on the composition, distribution, and kinematics of dust, metals, and gas in and around the star-forming regions of the galaxies. As the various baryons move in the ISM they will absorb photons emitted by the stellar populations of the galaxies at the launch velocity of the gas and at higher velocities of the gas as well (Martin & Bouché 2009; Steidel et al. 2010). How this gas is distributed and moves in the ISM and out into the IGM dictates the star-forming efficiency of galaxies and the column density of gas dictate the escape of ionizing radiation. Each of these properties can be probed by absorption lines in the rest-UV spectra of galaxies. This has been done extensively for higher mass samples where the UV continuum

S/N is generally sufficient to measure the absorption features (Shapley et al. 2003; Du et al. 2018; Jones et al. 2012; Sugahara et al. 2019; Harikane et al. 2020). However, even in these higher mass samples stacking is often used to measure the behavior of the "typical" galaxy at a given mass, or for a given property of the galaxy. Even with lensing the S/N of the UV continuum of our individual galaxies is insufficient to properly measure the absorption features. Because of this we choose to stack our galaxies as well and find that the HIS absorption lines are weaker than in the higher mass samples. We measure $\mathrm{EW_{HIS}} = -0.66$ Å and the literature values scatter tightly around $\mathrm{EW_{HIS}} = -1.4$ Å suggesting lower covering fractions of highly ionized ions. Additionally, the ratio of the SiIV lines in our sample is $\mathrm{EW_{SiIV1393}/EW_{SiIV1402}} = 2.07 \pm 0.28$, consistent with the HIS gas being optically thin. This implies a physical picture of a uniform screen of ionized gas around the star forming regions. Furthermore, with optically thin gas we are probing the column density of the gas with the EW of the lines instead of the covering fraction. The velocity offset from systemic for the stack is consistent with higher mass samples (-323 ± 13 km s^{-1} vs. -220^{+150}_{-100} km s^{-1}) suggesting that the velocities of HIS absorbing regions of the ISM are independent of the stellar mass of the galaxy. This may suggest that the ionized gas of the ISM is more likely to be ejected from dwarf galaxies than for higher mass star-forming galaxies.

The neutral hydrogen gas of the ISM can be traced using the absorption lines of ions with ionization potentials below that of Hydrogen. These ions primarily exist in regions of the ISM that are "shielded" by large column densities of neutral hydrogen, such that the harder radition from the stellar populations doesn't reach them. These lines have been used to confirm the picket fence model (Quider et al. 2009; Vasei et al. 2016), to probe

the velocities of outflowing gas (Shapley et al. 2003; Steidel et al. 2010; Jones et al. 2012; Hashimoto et al. 2013; Du et al. 2018; Sugahara et al. 2019), and to constrain the Lyα EW (Du et al. 2018; Jones et al. 2012; Berry et al. 2012; Shibuya et al. 2014; Saldana-Lopez et al. 2022). Because the LIS absorption lines can be used to trace the covering fraction of neutral hydrogen they are also correlated with the escape of Lyα and LyC photons (Saldana-Lopez et al. 2023). For dwarf galaxies at $z \sim 2$ the strength of the LIS absorption lines decreases relative to higher mass samples ($EW_{LIS} = -0.95 \pm 0.03$Å vs. $EW_{LIS} \sim -2$Å). Additionally, for our sample of dwarf galaxies the strength of the silicon lines show $EW_{SiII1260}/EW_{SiII1526} = 0.8 \pm 0.1$, consistent with the LIS gas being optically thick. This implies that lower mass galaxies generally have lower covering fractions of neutral hydrogen and likely have greater amounts of escaping ionizing radiation. This agrees with the analysis of Saldana-Lopez et al. (2023) who show that low-mass galaxies at higher redshift ($z \sim 3-5$) have lower covering fractions of LIS absorobing ions, higher Lyα escape fractions, and higher LyC escape fractions. We note that the average galaxy in their low-mass bin is a LAE and therefore may be biased towards strong line-emitters. Nevertheless, for our complete sample of dwarf galaxies we conclude that higher Lyα EWs are observed with lower LIS absorption line EWs.

We have presented a first look at the UV spectroscopy of a representative sample of dwarf galaxies at $z \sim 2$. While other samples have looked at the rest-UV spectroscopy of star-forming galaxies they have either been at higher masses ($\log(M^*/M_\odot) > 9$) or have been biased towards strong line emitters. Thanks to lensing we have been able to take spectroscopy of galaxies down to the faintest magnitudes possible from the ground.

We've shown that there are greater numbers of LAEs, the Lyα volumetric escape fraction is $\sim 5\%$, low- and high-ion absorption is weaker by about a factor of two in dwarf galaxies, and the typical dwarf galaxy will have Lyα in emission. Nevertheless, observing the faint universe is a difficult endeavor. In order to have a complete sample we required the use of the rest-optical emission lines from our Keck/MOSFIRE observations. However, because these observations are taken from the ground, emission lines are regularly obscured by contamination from the sky. The newly launched James Webb Space Telescope (JWST) can alleviate this complication as its NIR spectrometer covers the same wavelength range as MOSFIRE, and since it is in space it does not suffer from contamination from the sky. Data from JWST in conjunction with our existing rest-UV spectroscopy could increase our sample size by a factor of 5 or more. This improvement on the statistics of this sample would solidify many of our results which we can only marginally observe in this sample. For our measurements of the LIS and HIS absorption lines we were greatly limited by the sensitivity of our measurements of the UV-continuum. The suite of upcoming 30m telescopes will provide increased sensitivity for spectroscopic observations which may allow us to measure the LIS and HIS absorption EWs of individual dwarf galaxies at $z \sim 2$. As these data become available, this work will serve as a benchmark for future studies.

Bibliography

Adams, J. J., Blanc, G. A., Hill, G. J., et al. 2011, The hetdex pilot survey. I. Survey design, performance, and catalog of emission-line galaxies, doi: 10.1088/0067-0049/192/1/5

Alavi, A., Siana, B., Richard, J., et al. 2014, , 780, 143, doi: 10.1088/0004-637X/780/2/143

—. 2016, , 832, 56, doi: 10.3847/0004-637x/832/1/56

Berry, M., Gawiser, E., Guaita, L., et al. 2012, , 749, doi: 10.1088/0004-637X/749/1/4

Blanc, G. A., Adams, J. J., Gebhardt, K., et al. 2011, , 736, 31, doi: 10.1088/0004-637X/736/1/31

Bolton, J. S., & Haehnelt, M. G. 2013, , 429, 1695, doi: 10.1093/mnras/sts455

Bouwens, R. J., Illingworth, G. D., Ellis, R. S., Oesch, P. A., & Stefanon, M. 2022, arXiv e-prints, arXiv:2205.11526. https://arxiv.org/abs/2205.11526

Bruzual, G., & Charlot, S. 2003, , 344, 1000, doi: 10.1046/j.1365-8711.2003.06897.x

Cardelli, J. A., Clayton, G. C., & Mathis, J. S. 1989, , 345, 245, doi: 10.1086/167900

Carnall, A. C., McLure, R. J., Dunlop, J. S., & Davé , R. 2018, , 480, 4379, doi: 10.1093/mnras/sty2169

Caruana, J., Bunker, A. J., Wilkins, S. M., et al. 2014, , 443, 2831, doi: 10.1093/mnras/stu1341

Caruana, J., Wisotzki, L., Herenz, E. C., et al. 2018, , 473, 30, doi: 10.1093/mnras/stx2307

Cassata, P., Tasca, L. A., Le Fèvre, O., et al. 2015, , 573, 1, doi: 10.1051/0004-6361/201423824

Chabrier, G. 2003, , 115, 763, doi: 10.1086/376392

Ciardullo, R., Zeimann, G. R., Gronwall, C., et al. 2014, , 796, 64, doi: 10.1088/0004-637X/796/1/64

Claeyssens, A., Richard, J., Blaizot, J., et al. 2022, , 666, A78, doi: 10.1051/0004-6361/202142320

Cullen, F., McLure, R. J., Dunlop, J. S., et al. 2020, , 495, 1501, doi: 10.1093/MNRAS/STAA1260

Curtis-Lake, E., McLure, R. J., Pearce, H. J., et al. 2012, , 422, 1425, doi: 10.1111/j.1365-2966.2012.20720.x

De Barros, S., Pentericci, L., Vanzella, E., et al. 2017, , 608, 123, doi: 10.1051/0004-6361/201731476

De La Vieuville, G., Pelló, R., Richard, J., et al. 2020, , 644, A39, doi: 10.1051/0004-6361/202037651

Dijkstra, M., Gronke, M., & Venkatesan, A. 2016, , 828, 71, doi: 10.3847/0004-637x/828/2/71

Du, X., Shapley, A. E., Reddy, N. A., et al. 2018, , 860, 75, doi: 10.3847/1538-4357/aabfcf

Du, X., Shapley, A. E., Topping, M. W., et al. 2021, , 920, 95, doi: 10.3847/1538-4357/ac1273

Emami, N., Siana, B., Alavi, A., et al. 2020, , 895, 116, doi: 10.3847/1538-4357/ab8f97

Emami, N., Siana, B., El-Badry, K., et al. 2021, , 922, 217, doi: 10.3847/1538-4357/ac1f8d

Endsley, R., Stark, D. P., Charlot, S., et al. 2020, MNRAS, 000, 1

Erb, D. K., Pettini, M., Steidel, C. C., et al. 2016, , 830, 52, doi: 10.3847/0004-637X/830/1/52

Flury, S. R., Jaskot, A. E., Ferguson, H. C., et al. 2022, , 930, 126, doi: 10.3847/1538-4357/ac61e4

Foreman-Mackey, D., Hogg, D. W., Lang, D., & Goodman, J. 2013, , 125, 306, doi: 10.1086/670067

Freeman, W. R., Siana, B., Kriek, M., et al. 2019, , 873, 102, doi: 10.3847/1538-4357/ab0655

Gburek, T., Siana, B., Alavi, A., et al. 2022, arXiv e-prints, arXiv:2208.05976, doi: 10.48550/arXiv.2208.05976

Gburek, T., Siana, B., Alavi, A., et al. 2019, , 887, 168, doi: 10.3847/1538-4357/ab5713

Gordon, K. D., Clayton, G. C., Misselt, K. A., Landolt, A. U., & Wolff, M. J. 2003, , 594, 279, doi: 10.1086/376774

Grazian, A., Giallongo, E., Gerbasi, R., et al. 2016, , 585, A48, doi: 10.1051/0004-6361/201526396

Gronwall, C., Ciardullo, R., Hickey, T., et al. 2007, , 667, 79, doi: 10.1086/520324

Guaita, L., Gawiser, E., Padilla, N., et al. 2010, , 714, 255, doi: 10.1088/0004-637X/714/1/255

Harikane, Y., Laporte, N., Ellis, R. S., & Matsuoka, Y. 2020, , 902, 117, doi: 10.3847/1538-4357/abb597

Haro, P. A., Espinosa, J. M. R., Muñoz-Tuñón, C., et al. 2018, , 478, 3740, doi: 10.1093/MNRAS/STY1106

Hashimoto, T., Ouchi, M., Shimasaku, K., et al. 2013, , 765, 70, doi: 10.1088/0004-637X/765/1/70

Hashimoto, T., Garel, T., Guiderdoni, B., et al. 2017, , 608, A10, doi: 10.1051/0004-6361/201731579

Hathi, N. P., Le Fèvre, O., Ilbert, O., et al. 2016, , 588, 26, doi: 10.1051/0004-6361/201526012

Hayes, M., Östlin, G., Schaerer, D., et al. 2010, Nature, 464, 562, doi: 10.1038/nature08881

Hayes, M., Östlin, G., Duval, F., et al. 2014, , 782, 6, doi: 10.1088/0004-637X/782/1/6

Hoag, A., Bradač, M., Huang, K., et al. 2019, , 878, 12, doi: 10.3847/1538-4357/ab1de7

Izotov, Y. I., Schaerer, D., Worseck, G., et al. 2020, , 491, 468, doi: 10.1093/mnras/stz3041

Jauzac, M., Richard, J., Limousin, M., et al. 2016, , 457, 2029, doi: 10.1093/mnras/stw069

Jones, T., Stark, D. P., & Ellis, R. S. 2012, , 751, 51, doi: 10.1088/0004-637X/751/1/51

Jones, T. A., Ellis, R. S., Schenker, M. A., & Stark, D. P. 2013, , 779, 52, doi: 10.1088/0004-637X/779/1/52

Jullo, E., Kneib, J.-P., Limousin, M., et al. 2007, New Journal of Physics, 9, 447, doi: 10.1088/1367-2630/9/12/447

Jung, I., Finkelstein, S. L., Dickinson, M., et al. 2020, , 904, 144, doi: 10.3847/1538-4357/abbd44

Keerthi Vasan G., C., Jones, T., Sanders, R. L., et al. 2022, arXiv e-prints, arXiv:2209.05508, doi: 10.48550/arXiv.2209.05508

Konno, A., Ouchi, M., Nakajima, K., et al. 2016, , 823, 20, doi: 10.3847/0004-637x/823/1/20

Kornei, K. A., Shapley, A. E., Erb, D. K., et al. 2010, , 711, 693, doi: 10.1088/0004-637X/711/2/693

Kriek, M., Van Dokkum, P. G., Labbé, I., et al. 2009, , 700, 221, doi: 10.1088/0004-637X/700/1/221

Kroupa, P. 2004, , 48, 47, doi: 10.1016/j.newar.2003.11.007

Kusakabe, H., Blaizot, J., Garel, T., et al. 2020, , 638, A12, doi: 10.1051/0004-6361/201937340

Le Fèvre, O., Tasca, L. A. M., Cassata, P., et al. 2015, , 576, A79, doi: 10.1051/0004-6361/201423829

Leclercq, F., Bacon, R., Wisotzki, L., et al. 2017, , 608, A8, doi: 10.1051/0004-6361/201731480

Leitet, E., Bergvall, N., Hayes, M., Linné, S., & Zackrisson, E. 2013, , 553, A106, doi: 10.1051/0004-6361/201118370

Limousin, M., Richard, J., Jullo, E., et al. 2007, , 668, 643, doi: 10.1086/521293

Limousin, M., Richard, J., Jullo, E., et al. 2016, , 588, A99, doi: 10.1051/0004-6361/201527638

Lowenthal, J. D., Koo, D. C., Guzman, R., et al. 1997, , 481, 673, doi: 10.1086/304092

Lujan Niemeyer, M., Bowman, W. P., Ciardullo, R., et al. 2022, , 934, L26, doi: 10.3847/2041-8213/ac82e5

Martin, C. L., & Bouché, N. 2009, , 703, 1394, doi: 10.1088/0004-637X/703/2/1394

Mason, C. A., Treu, T., Dijkstra, M., et al. 2018, , 856, 2, doi: 10.3847/1538-4357/aab0a7

Matsuda, Y., Yamada, T., Hayashino, T., et al. 2012, , 425, 878, doi: 10.1111/j.1365-2966.2012.21143.x

Matthee, J., Sobral, D., Oteo, I., et al. 2016, , 458, 449, doi: 10.1093/MNRAS/STW322

Matthee, J., Naidu, R. P., Pezzulli, G., et al. 2021a, MNRAS, 000, 1

Matthee, J., Sobral, D., Hayes, M., et al. 2021b, MNRAS, 000, 1

McLean, I. S., Steidel, C. C., Epps, H., et al. 2010, in Society of Photo-Optical Instrumentation Engineers (SPIE) Conference Series, Vol. 7735, Ground-based and Airborne Instrumentation for Astronomy III, ed. I. S. McLean, S. K. Ramsay, & H. Takami, 77351E, doi: 10.1117/12.856715

McLean, I. S., Steidel, C. C., Epps, H. W., et al. 2012, in Society of Photo-Optical Instrumentation Engineers (SPIE) Conference Series, Vol. 8446, Ground-based and Airborne Instrumentation for Astronomy IV, ed. I. S. McLean, S. K. Ramsay, & H. Takami, 84460J, doi: 10.1117/12.924794

Mesinger, A., Aykutalp, A., Vanzella, E., et al. 2015, , 446, 566, doi: 10.1093/mnras/stu2089

Muratov, A. L., Kereš, D., Faucher-Giguère, C.-A., et al. 2015, , 454, 2691, doi: 10.1093/mnras/stv2126

Oke, J. B., & Gunn, J. E. 1983, , 266, 713, doi: 10.1086/160817

Oke, J. B., Cohen, J. G., Carr, M., et al. 1995, , 107, 375, doi: 10.1086/133562

Ono, Y., Ouchi, M., Mobasher, B., et al. 2012, , 744, 83, doi: 10.1088/0004-637X/744/2/83

Oyarzún, G. A., Blanc, G. A., González, V., Mateo, M., & Bailey, J. I. 2017, , 843, 133, doi: 10.3847/1538-4357/aa7552

Pahl, A. J., Shapley, A., Faisst, A. L., et al. 2020, , 493, 3194, doi: 10.1093/mnras/staa355

Partridge, R. B., & Peebles, P. J. E. 1967, , 147, 868, doi: 10.1086/149079

Pentericci, L., Fontana, A., Vanzella, E., et al. 2011, , 743, doi: 10.1088/0004-637X/743/2/132

Priewe, J., Williams, L. L. R., Liesenborgs, J., Coe, D., & Rodney, S. A. 2017, , 465, 1030, doi: 10.1093/mnras/stw2785

Prochaska, J. X., Hennawi, J. F., Westfall, K. B., et al. 2020, arXiv e-prints, arXiv:2005.06505. https://arxiv.org/abs/2005.06505

Prochaska, J. X., Hennawi, J. F., Westfall, K. B., et al. 2020, Journal of Open Source Software, 5, 2308, doi: 10.21105/joss.02308

Prochaska, J. X., Hennawi, J., Cooke, R., et al. 2020, pypeit/PypeIt: Release 1.0.0, v1.0.0, Zenodo, doi: 10.5281/zenodo.3743493

Pucha, R., Reddy, N. A., Dey, A., et al. 2022, , 164, 159, doi: 10.3847/1538-3881/ac83a9

Quider, A. M., Pettini, M., Shapley, A. E., & Steidel, C. C. 2009, , 398, 1263, doi: 10.1111/j.1365-2966.2009.15234.x

Quider, A. M., Shapley, A. E., Pettini, M., Steidel, C. C., & Stark, D. P. 2010, , 402, 1467, doi: 10.1111/j.1365-2966.2009.16005.x

Reddy, N. A., & Steidel, C. C. 2009, , 692, 778, doi: 10.1088/0004-637X/692/1/778

Reddy, N. A., Steidel, C. C., Pettini, M., et al. 2008, Supplement Series, 175, 48, doi: 10.1086/521105

Reddy, N. A., Topping, M. W., Shapley, A. E., et al. 2022, , 926, 31, doi: 10.3847/1538-4357/ac3b4c

Rudie, G. C., Steidel, C. C., Pettini, M., et al. 2019, , 885, 61, doi: 10.3847/1538-4357/ab4255

Rutkowski, M. J., Scarlata, C., Henry, A., et al. 2017, , 841, L27, doi: 10.3847/2041-8213/aa733b

Saldana-Lopez, A., Schaerer, D., Chisholm, J., et al. 2022, , 663, A59, doi: 10.1051/0004-6361/202141864

—. 2023, , doi: 10.1093/mnras/stad1283

Sanders, R. L., Shapley, A. E., Jones, T., et al. 2021, , 914, 19, doi: 10.3847/1538-4357/abf4c1

Schenker, M. A., Stark, D. P., Ellis, R. S., et al. 2012, , 744, 179, doi: 10.1088/0004-637X/744/2/179

Senchyna, P., Stark, D. P., Vidal-García, A., et al. 2017, , 472, 2608, doi: 10.1093/mnras/stx2059

Shapley, A. E., Steidel, C. C., Pettini, M., & Adelberger, K. L. 2003, , 588, 65, doi: 10.1086/373922

Shibuya, T., Ouchi, M., Nakajima, K., et al. 2014, , 788, 74, doi: 10.1088/0004-637X/788/1/74

Shivaei, I., Reddy, N. A., Siana, B., et al. 2018, , 855, 42, doi: 10.3847/1538-4357/aaad62

Siana, B., Teplitz, H. I., Ferguson, H. C., et al. 2010, , 723, 241, doi: 10.1088/0004-637X/723/1/241

Snapp-Kolas, C., Siana, B., Gburek, T., et al. 2022, arXiv e-prints, arXiv:2211.00041, doi: 10.48550/arXiv.2211.00041

Sobral, D., & Matthee, J. 2019, , 623, doi: 10.1051/0004-6361/201833075

Sobral, D., Matthee, J., Best, P., et al. 2017, , 466, 1242, doi: 10.1093/mnras/stw3090

Sparre, M., Hayward, C. C., Feldmann, R., et al. 2017, , 466, 88, doi: 10.1093/mnras/stw3011

Stark, D. P., Ellis, R. S., Chiu, K., Ouchi, M., & Bunker, A. 2010, , 408, 1628, doi: 10.1111/j.1365-2966.2010.17227.x

Stark, D. P., Ellis, R. S., & Ouchi, M. 2011, , 728, 2, doi: 10.1088/2041-8205/728/1/L2

Steidel, C. C., Erb, D. K., Shapley, A. E., et al. 2010, , 717, 289, doi: 10.1088/0004-637X/717/1/289

Steidel, C. C., Giavalisco, M., Pettini, M., Dickinson, M., & Adelberger, K. L. 1996, , 462, doi: 10.1088/1538-4357/462/1/l17

Sugahara, Y., Ouchi, M., Harikane, Y., et al. 2019, , 886, 29, doi: 10.3847/1538-4357/ab49fe

Sugahara, Y., Ouchi, M., Lin, L., et al. 2017, , 850, 51, doi: 10.3847/1538-4357/aa956d

Trainor, R. F., Steidel, C. C., Strom, A. L., & Rudie, G. C. 2015, , 809, 89, doi: 10.1088/0004-637X/809/1/89

Trainor, R. F., Strom, A. L., Steidel, C. C., et al. 2019, , 887, 85, doi: 10.3847/1538-4357/ab4993

Vanzella, E., Guo, Y., Giavalisco, M., et al. 2012, , 751, 70, doi: 10.1088/0004-637X/751/1/70

Vasei, K., Siana, B., Shapley, A. E., et al. 2016, , 831, 38, doi: 10.3847/0004-637X/831/1/38

Verhamme, A., Orlitová, I., Schaerer, D., & Hayes, M. 2015, , 578, A7, doi: 10.1051/0004-6361/201423978

Verhamme, A., Orlitová, I., Schaerer, D., et al. 2017, , 597, A13, doi: 10.1051/0004-6361/201629264

Wardlow, J. L., Malhotra, S., Zheng, Z., et al. 2014, , 787, doi: 10.1088/0004-637X/787/1/9

Weiss, L. H., Bowman, W. P., Ciardullo, R., et al. 2021, , 920, 95, doi: 10.3847/1538-4357/ac1273

Weldon, A., Reddy, N. A., Topping, M. W., et al. 2022, , 515, 841, doi: 10.1093/mnras/stac1822

Yang, H., Malhotra, S., Gronke, M., et al. 2017, , 844, 171, doi: 10.3847/1538-4357/aa7d4d

Zhang, Y., Ouchi, M., Gebhardt, K., et al. 2021, , 922, 167, doi: 10.3847/1538-4357/ac1e97